12-13-2011

Paleomagnetic constraints on deformation of superfast-spread oceanic crust exposed at Pito Deep Rift

Andrew J. Horst
Marshall University, horsta@marshall.edu

R. J. Varga

J. S. Gee

J. A. Karson

Recommended Citation
Horst, A. J., R. J. Varga, J. S. Gee, and J. A. Karson (2011), Paleomagnetic constraints on deformation of superfast- spread oceanic crust exposed at Pito Deep Rift, J. Geophys. Res., 116, B12103, doi:10.1029/2011JB008268.

Paleomagnetic constraints on deformation of superfast-spread oceanic crust exposed at Pito Deep Rift

A. J. Horst,[1] R. J. Varga,[2] J. S. Gee,[3] and J. A. Karson[1]

Received 28 January 2011; revised 7 September 2011; accepted 11 September 2011; published 13 December 2011.

[1] The uppermost oceanic crust produced at the superfast spreading (~142 km Ma^{-1}, full-spreading rate) southern East Pacific Rise (EPR) during the Gauss Chron is exposed in a tectonic window along the northeastern wall of the Pito Deep Rift. Paleomagnetic analysis of fully oriented dike (62) and gabbro (5) samples from two adjacent study areas yield bootstrapped mean remanence directions of 38.9° ± 8.1°, −16.7° ± 15.6°, n = 23 (Area A) and 30.4° ± 8.0°, −25.1° ± 12.9°, n = 44 (Area B), both are significantly distinct from the Geocentric Axial Dipole expected direction at 23° S. Regional tectonics and outcrop-scale structural data combined with bootstrapped remanence directions constrain models that involve a sequence of three rotations that result in dikes restored to subvertical orientations related to (1) inward-tilting of crustal blocks during spreading (Area A = 11°, Area B = 22°), (2) clockwise, vertical-axis rotation of the Easter Microplate (A = 46°, B = 44°), and (3) block tilting at Pito Deep Rift (A = 21°, B = 10°). These data support a structural model for accretion at the southern EPR in which outcrop-scale faulting and block rotation accommodates spreading-related subaxial subsidence that is generally less than that observed in crust generated at a fast spreading rate exposed at Hess Deep Rift. These data also support previous estimates for the clockwise rotation of crust adjacent to the Easter Microplate. Dike sample natural remanent magnetization (NRM) has an arithmetic mean of 5.96 A/m ± 3.76, which suggests that they significantly contribute to observed magnetic anomalies from fast- to superfast-spread crust.

Citation: Horst, A. J., R. J. Varga, J. S. Gee, and J. A. Karson (2011), Paleomagnetic constraints on deformation of superfast-spread oceanic crust exposed at Pito Deep Rift, *J. Geophys. Res.*, *116*, B12103, doi:10.1029/2011JB008268.

1. Introduction

[2] Subaxial processes that operate beneath fast and superfast spreading ridges during crustal construction cannot be observed directly, and are typically inferred from ophiolite studies, seafloor-surface geological and geophysical observations. Constraints on magmatic accretion, mechanical deformation, and hydrothermal alteration processes are determined from the internal geologic structure of ophiolites [*Moores and Vine*, 1971; *Penrose Conference Participants*, 1972; *Cann*, 1974; *Casey et al.*, 1981; *Varga and Moores*, 1985; *Nicolas*, 1989], marine seismic studies [*Christeson et al.*, 1992; *Detrick et al.*, 1993; *Kent et al.*, 1994; *Hallenborg et al.*, 2003], and limited deep crustal drilling [*Alt et al.*, 1993; *Pockalny and Larson*, 2003; *Tivey et al.*, 2005; *Wilson et al.*, 2006]. Additional constraints come from studies of dike intrusion events [*Delaney et al.*, 1998; *Perfit and Chadwick*, 1998], and eruptions along modern spreading centers [*Soule et al.*, 2009, and references therein]. Detailed bathymetric and geochemical data along modern fast spreading ridges like the East Pacific Rise (EPR) also contribute to current understanding of crustal accretion at fast- to superfast spreading ridges, however, direct observations along seafloor escarpments (tectonic windows) [*Karson*, 1998, 2002], provide the only prospect to observe oceanic crust in situ in three-dimensions.

[3] Tectonic windows into the oceanic crust provide the opportunity to directly investigate structural, magnetic, and compositional aspects of extensive exposures of the upper oceanic crust in situ from which to infer spreading processes [*Francheteau et al.*, 1990; *Karson*, 1998; *Tivey et al.*, 1998; *Karson et al.*, 2002a, 2002b; *Varga et al.*, 2004; *Larson et al.*, 2005; *Pollock et al.*, 2005; *Hayman and Karson*, 2007]. Investigations of tectonic windows and drill cores confirm a generalized layered sequence of rock types for crust formed at intermediate to fast spreading rates that consists of basaltic lavas overlying a sheeted dike complex underlain by massive gabbro, and reveal similar structural relationships [*Karson*, 2002]. These studies indicate broadly similar uppermost crustal structure with lava flows that typically dip inward (toward the ridge axis) and increase in dip magnitude with depth, while individual and sheeted dikes commonly dip outward (away from the ridge axis). These observations are interpreted in terms of subaxial subsidence

[1]Department of Earth Sciences, Syracuse University, Syracuse, New York, USA.
[2]Geology Department, Pomona College, Claremont, California, USA.
[3]Scripps Institution of Oceanography, University of California, San Diego, La Jolla, California, USA.

0148-0227/11/2011JB008268

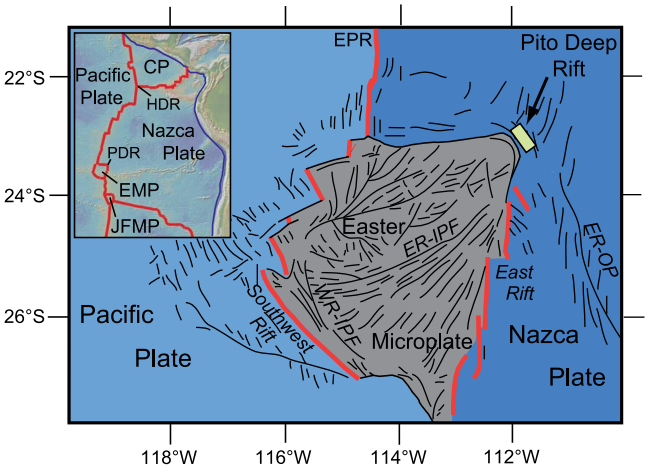

Figure 1. Tectonic map of the Easter Microplate (EMP) and Pito Deep Rift (PDR) with East Pacific Rise (EPR) inset location map. Thin black lines represent bathymetric lineaments based on the GLORIA data [after *Rusby and Searle*, 1995], and thick red and black lines show plate boundaries. HDR, Hess Deep Rift; CP, Cocos plate; JFMP, Juan Fernandez Microplate; WR-IPF, West Rift inner pseudofault; ER-IPF, East Rift inner pseudofault; ER-OP, East Rift outer pseudofault.

that accommodates thickening of lavas that accumulate within a very narrow (~2 km), low-relief region at the ridge axis [*Karson*, 2002]. Dikes are typically not vertical, but could be intruded in non-vertical orientations, or rotated from their original orientations; this requires an independent assessment of intrusion geometry and any subsequent rotations.

[4] In order to extend these observations to uppermost crust generated at superfast spreading rates, a study was conducted at the Pito Deep Rift. Faulting at the tip of the northward-propagating rift exposes superfast-spread (~142 km Ma^{-1}, full-rate [*Hey et al.*, 1995]) crust generated at the southern EPR (Figure 1). Crust at two focused study areas (Area A and B) at Pito Deep Rift was generated at the EPR ~3 Ma and span normal polarity Chron C2An.2n and Chron C2An.3n, respectively (Figure 2). Extensive cliffs orientated at a high angle to spreading-related structures and isochrons expose a sequence of basalt lavas, a lava/dike transition zone, sheeted dikes, and massive gabbro. Dikes within the sheeted dike complex at Pito Deep Rift dip primarily to the southeast, that is outward from the EPR, with dips varying from 90° to 46°. Cataclastic fault zones primarily focused between individual dikes or separating panels of subparallel dikes, suggest an inseparable kinematic relationship of the damage zones and the tilting of dikes [*Karson et al.*, 2005; *Hayman and Karson*, 2009; L. A. Chutas, Structures in upper oceanic crust: Perspectives from Pito Deep and Iceland, unpublished Masters thesis, 122 pp., Duke University, 2007]. The mechanical anisotropy of the uppermost crust imparted by subparallel dikes and faults provides planes of weakness that preferentially slip allowing tilting to occur, similar to block rotations in other extensional settings including ophiolites and other tectonic windows [*Varga*, 1991; *Varga et al.*, 1999, 2004]. Observations of rare vertical dikes cross-cutting this assemblage of inward-tilted lavas and sheeted dikes suggest the total accumulated thickness of lava and significant tilting of uppermost crustal units all occurred in a narrow zone (~2 km) beneath the ridge axis. A similar uppermost crustal structure occurs in the Equatorial Pacific in crust formed at a spreading rate of 135 km Ma^{-1} [*Lonsdale*, 1988] at Hess Deep Rift [*Karson et al.*, 2002a; *Varga et al.*, 2004]. The lack of volcanic constructional relief (<~200 m), and the structure of lava flows that generally increase in dip toward the ridge axis with depth imply significant (≥400 m) creation of accommodation space created by subaxial subsidence that occurs at or within ~2 km of the ridge axis [*Karson*, 2002; *Karson et al.*, 2002a, 2002b]. Thus it appears that coordinated faulting and block rotation are integral parts of crustal accretion processes at intermediate- to fast spreading ridges and Pito Deep Rift presents an opportunity to evaluate these processes at superfast spreading ridges.

[5] In this paper we present results from structural relationships and paleomagnetic remanence directions of a set of fully oriented block samples of basalt dikes and massive gabbros collected from the Pito Deep Rift in the southeast Pacific. These data form constraints on processes of subaxial subsidence, and indicate significant clockwise rotation related to coupling between the Nazca Plate and adjacent Easter Microplate, as well as an additional tilting related to the opening of the Rift. The constraints on the construction and deformation of oceanic crust generated at superfast spreading rates are similar to and augment results from Hole 1256D, drilled into 15 Ma superfast-spread crust of the Cocos Plate. In addition, these results have significant implications for magnetic anomaly intensity and anomalous skewness. The natural remanent magnetization (NRM) from dike samples suggests that dikes significantly contribute to observed magnetic anomalies from fast- to superfast-spread crust. Our interpretation of the rotational history that includes inward-tilting near the ridge axis would produce the opposite sense of anomalous skewness to that observed, a distinction that could be reconciled a couple of different ways as discussed later. Although a subset of the data was reported by *Varga et al.* [2008], the full data set and thorough analysis is presented here.

2. Tectonic Window at Pito Deep Rift

[6] Along the southern EPR at ~23°S, Pito Deep Rift represents the amagmatic tip of the northward-propagating East Ridge along the northeastern boundary of the Easter Microplate (Figures 1 and 2). The steep, fault-bounded, NW/SE-trending escarpments of Pito Deep Rift have >4000 m of relief and expose oceanic crust accreted ~3 Ma ago along a superfast spreading segment of the N/S trending, southern EPR (~142 km Ma^{-1}, full-rate [*Hey et al.*, 1995]). Major fault scarps along the rift walls oriented at a high angle to spreading-generated structures provide an ideal cross-sectional view of the upper oceanic crust. Although most of the structures exposed in the escarpment appear to be related to spreading processes at the EPR [e.g., *Hayman and Karson*, 2009], overprinting of ridge-related structures is related to the tectonic evolution of the Easter Microplate and rifting of Pito Deep [*Engeln and Stein*, 1984; *Hey et al.*,

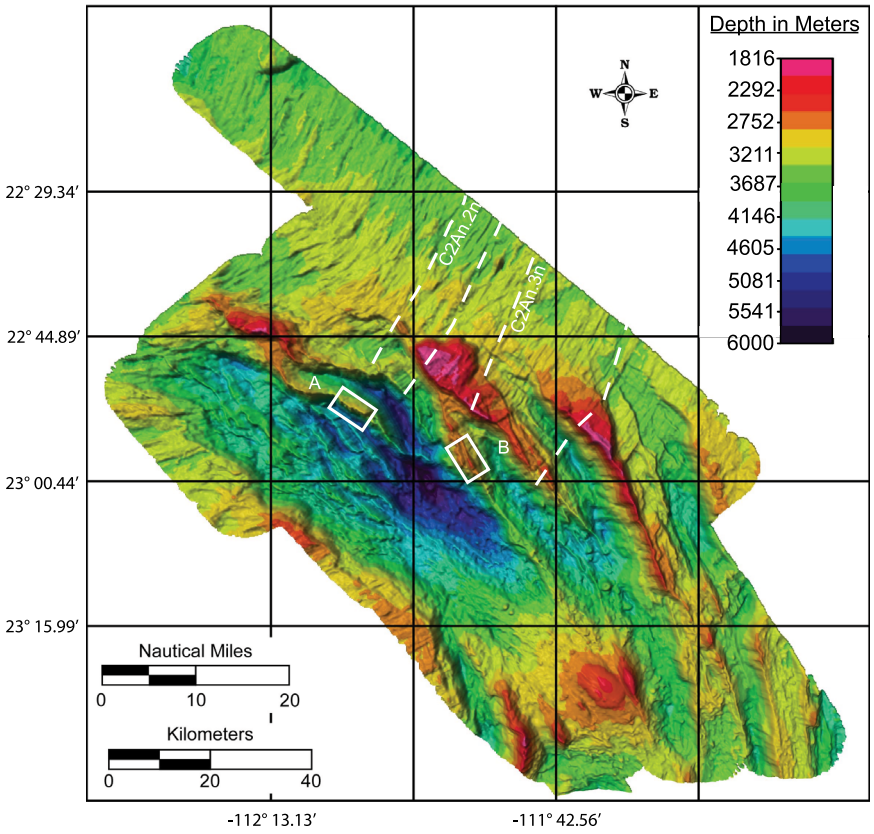

Figure 2. SeaBeam2000 bathymetry with highlighted study Areas A and B shown in white boxes [*Karson et al.*, 2005]. White dashed lines show polarity boundaries for Chron C2An.2n (3.110–3.220 Ma) and Chron C2An.3n (3.330–3.580 Ma) [*Cande and Kent*, 1995].

1985; *Schilling et al.*, 1985; *Searle et al.*, 1989; *Naar and Hey*, 1991; *Schouten et al.*, 1993; *Searle et al.*, 1993; *Rusby and Searle*, 1995; *Hey et al.*, 2002].

[7] The crust exposed on the northeastern scarp of the Pito Deep Rift appears to have a complicated history involving the clockwise rotation of the Easter Microplate in addition to rifting associated with the northward propagation of the East Ridge [*Hey et al.*, 1985; *Searle et al.*, 1989; *Martinez et al.*, 1991; *Naar and Hey*, 1991; *Rusby and Searle*, 1995]. Both bathymetric and magnetic anomaly lineations [*Naar and Hey*, 1991; *Naar et al.*, 1991; *Varga et al.*, 2008] reveal trends that deviate from EPR-parallel trends by 020° to 045° clockwise near the northeastern wall of Pito Deep Rift (Figure 2). Trends of abyssal hill lineations approach 055° to 065° near the dive areas, and trend ~070° across the rift to the southwest, in the interior of the microplate. However, to the west of the present EPR axis, crust of the Pacific Plate corresponding to the same age as that exposed at Pito Deep Rift shows magnetic anomaly and abyssal hill lineaments that nearly parallel the current approximately N/S EPR axis [*Naar and Hey*, 1991]. Therefore, the crust and the NE-SW striking faults and fractures of the northeast wall of the Pito Deep Rift in the study areas are interpreted as spreading-related structures that have been rotated clockwise. Although the structural relationships of upper crustal units described were initially created during seafloor spreading, they have likely been modified by the rotation of the Easter Microplate and rifting of Pito Deep.

[8] A previous paleomagnetic investigation of oriented samples from locations within the interior and around the boundaries of the Easter Microplate suggested a significant (48.5° ± 11°) clockwise vertical-axis rotation [*Cogné et al.*, 1995]; however, the 7 samples included in the analysis were collected from 4 different widely spaced (>100 km apart) sites within the Easter Microplate to the southwest of Pito Deep Rift which would contribute to considerable uncertainty and it is likely that this previous uncertainty estimate is unrealistically small. An estimate of ~61° of vertical-axis rotation was suggested by *Varga et al.* [2008] from a smaller subset of the data presented in this paper. In this paper we present the full data set with a more rigorous statistical assessment of the rotational history that generally supports this earlier estimate of a large component of vertical-axis rotation. However, here we also argue that the remanence directions are typically shallower than expected and can be explained by an additional tilt related to the opening of Pito Deep Rift. We also discuss these paleomagnetic data in relationship to magnetization of oceanic crust.

3. Internal Structure of Major Rock Units of the Northeastern Wall of the Rift

[9] Integrated investigations with the submersible *Alvin*, remotely operated vehicle (ROV) *Jason II*, and DSL-120

side-scan sonar provide details of the internal structure of the upper crustal units of the seafloor within two study Areas, A and B (Figure 2). Total outcrop width (parallel to the spreading direction) covered by *Alvin* and *Jason II* transects is approximately 4 km in each area. Assuming a constant half-spreading rate of 71 km Ma^{-1}, the combined investigation of these two areas represents ~100 ka of spreading. Fifteen transects of the escarpment using *Alvin* and *Jason II* together with the earlier *Nautile* Dives, reveal the structure of the uppermost crust within both areas (Figure 3) [*Karson*, 2005; Chutas, unpublished thesis, 2007]. The rock units mapped during this nested-scale survey along the northeast wall of the Pito Deep Rift are similar to those described from upper crustal levels of ophiolites [*Moores and Vine*, 1971; *Casey et al.*, 1981; *Nicolas*, 1989], drill cores [*Alt et al.*, 1996; *Wilson et al.*, 2006], and other seafloor escarpments [*Karson et al.*, 2002a, 2002b].

3.1. Basaltic Lava Flows

[10] The upper portion of the escarpment exposes extensive outcrops of variably fractured and faulted basaltic lavas with a range in unit thickness between 200 and 500 m (Chutas, unpublished thesis, 2007). Pillow lava morphologies constitute much of the unit with very few lobate or tabular sheet flows (Figure 4). Although rare, lobate and tabular flows appear weakly deformed and nearly horizontal near the top of the lava unit and increase in fracturing with depth. Contacts between the few lobate and tabular flows in the middle to lower parts of the unit have dips of approximately 10–40° to the northwest, inward and toward the EPR (Chutas, unpublished thesis, 2007).

[11] A transition zone occurs in the lowermost lavas, with basaltic dikes and swarms of dikes that cut the lavas increasing in proportion down-section. The boundary between these units is gradational and on average is approximately 200 m thick. This transition zone is ~50 m thicker than Hole 504B [*Anderson et al.*, 1982], and thicker than typically inferred from seismic data [*Hooft et al.*, 1996].

3.2. Sheeted Dike Complex

[12] The sheeted dike complex, with > 90% basaltic dikes, is composed of panels of subparallel dikes separated by fault zones or swarms of dikes (Figure 5). Individual dikes within dike swarms are typically ~1 m wide, but massive individual dikes up to 2 m wide are locally present. The vertical dimension of the unit ranges from 400 to 1000 m (Figure 3), and it exhibits a complex internal structure similar to that reported from previous studies at Hess Deep Rift, where both individual dikes and panels of dikes are typically not vertical [*Karson et al.*, 2002a; *Varga et al.*, 2004]. As opposed to parallel, vertical dikes commonly depicted in models of ridges derived from ophiolites [*Moores and Vine*, 1971; *Penrose Conference Participants*, 1972; *Casey et al.*, 1981; *Pallister*, 1981] and a few other seafloor escarpments [*Francheteau et al.*, 1992; *Karson*, 1998] dikes at Pito Deep Rift dominantly strike northeast, and have dips ranging from 90° to 46°, to the southeast, away from the EPR (Figure 6). In Area A, the average orientation of dikes measured with the Geocompass is 066°/83° SE, α_{95} = 9.3°, n = 25. Most of dikes in this area dip to the SE (average 069°/75° SE, α_{95} = 9.7°, n = 18), while ~1/3 of dikes dip to the NW (average 238°/75° NW, α_{95} = 12.6°, n = 7). In Area B, dikes have a more consistent orientation with an average of 054°/68° SE, α_{95} = 6.5°, n = 39. Overall, the average for dikes measured in both areas is 059°/74° SE, α_{95} = 5.7°, n = 64.

[13] High-temperature hydrothermal alteration in the sheeted dike complex is highly heterogeneous on scales of tens to hundreds of meters [*Heft et al.*, 2008]. The extent of alteration measured as the abundance of secondary minerals ranges from 0% to >80%. In general, the sheeted dike complex is relatively fresh, with an average of 27% alteration. Greenschist facies assemblages dominated by amphibole, with some interspersed chlorite-rich dikes reveal few systematic spatial trends or variations with depth, and no systematic pattern was observed between study Area A and B. These common assemblages indicate peak alteration temperatures ranging from <300°C to >450°C throughout the sheeted dike complex [*Heft et al.*, 2008].

3.3. Gabbroic Rocks

[14] Massive gabbroic rocks underlie the sheeted dike complex; however, the contact is typically covered with talus (Figure 7). Where exposed, the contact generally occurs over no more than a few tens of meters and has subdued relief at this scale of observation. Sparse subvertical dikes occur within the gabbro and are less faulted than in the overlying sheeted dike complex. The maximum thickness of the gabbroic material is > 700 m, but the base is not exposed in either study area [*Karson*, 2005].

[15] As documented by *Perk et al.* [2007], the uppermost plutonic rocks exhibit significant spatial heterogeneity, with a suite of samples that includes gabbros, olivine gabbros, troctolites, and anorthosite. In some gabbros collected >100 m below the sheeted dike complex minor crystal-plastic deformation is evident by plagioclase deformation twins, and undulose extinction and sub-grains in olivine. Qualitatively, a sample suite of 23 gabbros from Area B imply an increase in crystal-plastic deformation with depth [*Perk et al.*, 2007].

4. Sampling Methods, Laboratory Procedures, and Statistical Analyses

[16] A total of 62 basalt dike and 5 gabbro samples collected for paleomagnetic analysis by *Alvin* and ROV *Jason II* were fully oriented in situ using the Geocompass [*Hurst et al.*, 1994a; *Varga et al.*, 2004]. The strike and dip of two or more surfaces for each individual block were determined when the device was held flush against a rock surface. When recovered, each block was then restored to its outcrop orientation. The Geocompass and subsequent reorienting technique has demonstrated its utility and relative accuracy (±~10°) in previous studies of the Hess Deep Rift [*Karson et al.*, 1992; *Hurst et al.*, 1994a; *Varga et al.*, 2004], and on the Mid-Atlantic Ridge [*Lawrence et al.*, 1998]. A goal during several individual dives was to collect multiple independently oriented block samples from a coherent structural block in order to average orientation uncertainties and address scatter related to secular variation. Typically two to six fully oriented samples were collected from one small contiguous area during individual dive transects, with a maximum of fourteen samples collected during *Alvin* Dive 4081, and maximum of nine samples collected during *Jason* Dive transects. The few adjacent block samples collected

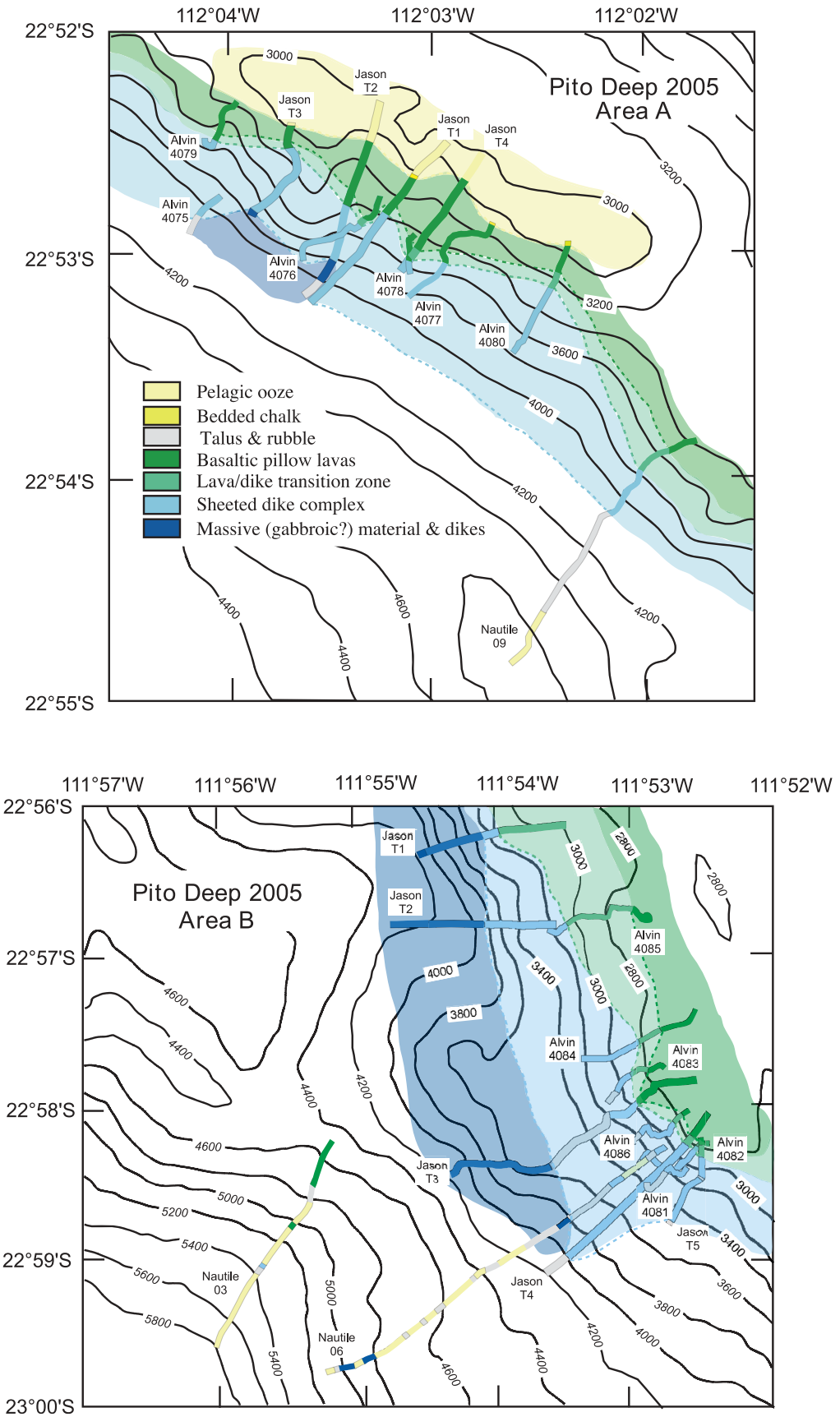

Figure 3. *Alvin* and *Jason II* transects in Areas A and B. Also shown are the *Nautile* Dive transects (after Chutas, unpublished thesis, 2007).

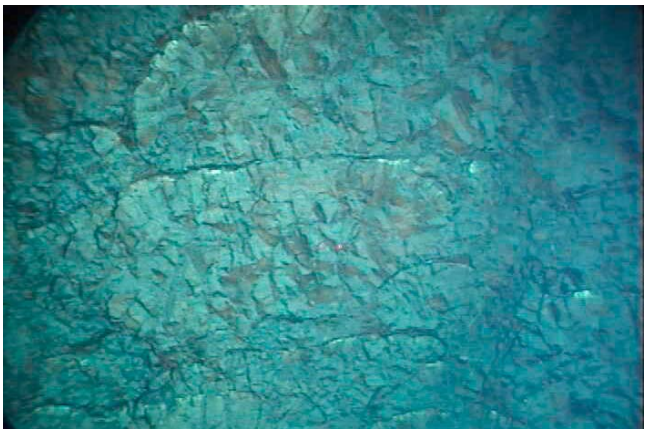

Figure 4. Pillow and lobate basaltic lavas with ~10° NW dip, toward the EPR. Field of view is to the northeast and approximately 3 m across. Image taken during *Alvin* dive 4077 in Area A at depth of ~3285 m.

during individual transects together are considered to be one paleomagnetic site. Collecting many closely spaced, independently oriented samples from one coherent structural block, such as along the *Alvin* Dive 4081 transect, reduces the uncertainty on the average remanence direction from this site. Sample remanence directions from individual *Alvin* or *Jason* dives are expected to be consistent, unless structural boundaries were crossed during the dive transect.

[17] Sample numbers (e.g., 812019), as reported here (Table 1), are a combination of truncated dive number (e.g., 81 = Dive 4081) and *Alvin* dive times (e.g., 2019 = 20:19 h) during individual dives. Samples collected using *Jason II* have a similar identification convention only with an abbreviated date replacing the dive number (e.g., 200830; 20 = 2/20/05; 0830 = 08:30 h). For most fully oriented block samples, 5 to 25, standard 2.54-cm diameter cores were drilled; some cores yielded more than one specimen (subcore). However, a few relatively small block samples yielded only two specimens.

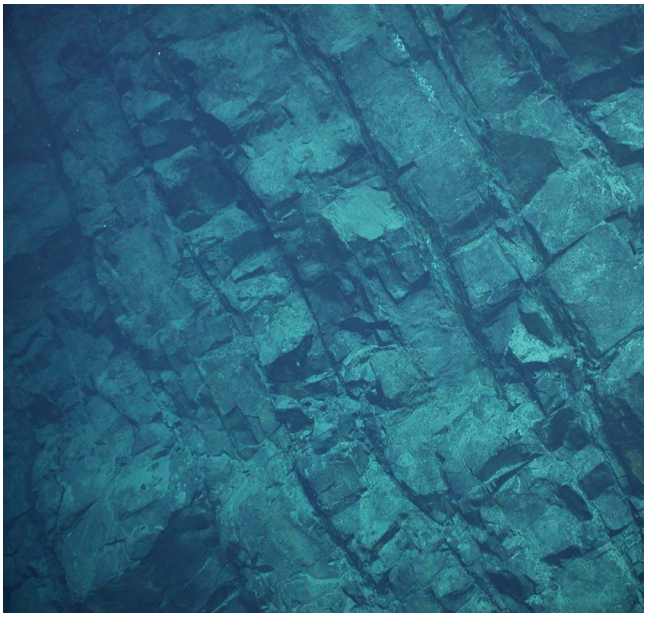

Figure 5. Typical view of sheeted dikes, with consistent SE dip, each dike is ~1 m wide. *Alvin* dive 4082 in Area B at depth of ~2948 m, view to northeast.

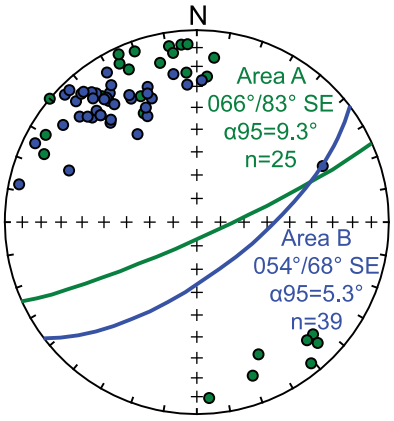

Figure 6. Equal-area lower hemisphere projection of all 64 poles to dike margins measured with Geocompass in Areas A and B. Total number of dikes measured with Geocompass includes 2 dikes in each area for which no oriented sample was collected. Mean dike orientations in Areas A and B are shown by great circles 066°/83° SE shown in green and 054°/68° SE shown in blue, respectively.

[18] Paleomagnetic remanence measurements and demagnetization were performed on a Molspin spinner magnetometer and other standard equipment at the College of Wooster, with some specimens measured on a 2G Enterprises cryogenic magnetometer in a shielded room at Scripps Institution of Oceanography. For most blocks, 4 to 7 specimens were progressively demagnetized using thermal or alternating field (AF) techniques. However, only 2 specimens were measured for some blocks generally due to their small size. All specimens were subjected to a complete spectrum of

Figure 7. Typical outcrop of massive gabbroic rock at Pito Deep Rift. Image taken during *Jason II* transect 3 in Area A at depth of 4168 m, view is to 050°.

Table 1. Paleomagnetic Results for Pito Deep Rift 2005 Oriented Dike and Gabbro Samples[a]

			Attitude[c]					Stability[d]								
Sample	Rock Type[b]	Depth (m)	Strike (deg)	Dip (deg)	N/Nc	NRM (A/m)	X, (μSI)	MDF′, (mT)	MDT′, (°C)	k	α95 (deg)	csd (deg)	D (deg)	I (deg)	Angle (deg)	Pol[c]
							AREA A									
090939	D	3903	024	76 SE	5 of 5	1.02	19551	14	522	491	3.5	3.7	20.7	−25.8	19.2	N
110038	D	3401	064	81 SE	5 of 5	9.17	21600	47	374	740	2.8	3.0	17.3	−12.0	21.4	N
110150	D	3342	065	86 SE	4 of 4	6.60	43173	36	271	421	4.5	3.9	14.2	57.3	76.8	U
110235	D	3273	053	71 SE	2 of 2	7.91	38934	34	492	645	9.8	3.2	26.2	−44.5	29.8	N
100532	D	3574	224	73 NW	6 of 6	2.52	65681	12	520	165	5.2	6.3	39.2	−50.7	34.0	N
100708	D	3592	245	65 NW	5 of 6	3.15	43123	12	551	930	2.5	2.7	51.9	−40.6	26.4	N
751832	D	3899	096	75 SW	6 of 6	1.78	66864	8	528	90	7.1	8.6	23.2	−17.9	15.0	N
751912	D	3826	085	82 SE	5 of 5	3.19	34116	10	546	754	2.8	2.9	218.0	46.9	30.2*	R
761740	D	3576	077	74 SE	5 of 5	1.87	18678	13	540	328	4.2	4.5	50.1	−15.1	10.9	N
761756	D	3557	081	82 SE	6 of 6	1.26	22550	12	552	261	4.2	5.0	192.1	−25.7	49.8*	U
761853	D	3445	266	81 NW	3 of 3	2.66	25265	14	554	376	6.4	4.2	60.5	−30.6	24.1	N
771643	D	3579	087	82 SE	4 of 4	3.09	53687	9	546	833	3.2	2.8	30.6	−25.6	11.8	N
771654	D	3575	064	53 SE	3 of 3	3.27	72327	12	542	2374	2.5	1.7	31.5	2.2	20.3	N
771715	D	3538	225	78 NW	3 of 4	2.90	40190	9	–	805	4.3	2.9	37.3	40.4	57.1	U
771718	D	3538	231	84 NW	5 of 6	2.61	44355	11	502	421	3.7	3.9	49.9	−39.3	24.6	N
771721	D	3538	227	73 NW	3 of 3	1.10	54648	14	276	186	9.1	5.9	37.3	−1.3	15.5	N
771931	D	3279	066	61 SE	6 of 6	6.22	30614	29	529	3413	1.1	1.4	39.3	−38.2	21.5	N
781709	D	3561	040	90	7 of 7	1.78	28806	18	358	564	2.5	3.4	67.4	−35.6	31.6	N
781903	D	3523	250	74 NW	4 of 4	4.46	41944	26	532	142	7.7	6.8	220.5	48.0	31.3*	R
782008	D	3344	070	84 SE	2 of 2	2.48	21832	30	521	10852	2.4	0.8	61.2	30.1	51.5	U
791616	D	3259	086	67 SE	4 of 4	14.99	58279	22	551	911	3.0	2.7	70.8	7.2	39.6	N
791723	D	3328	082	78 SE	2 of 2	10.74	49180	27	546	116	11.5	7.5	33.3	−13.6	6.2	N
791817	D	3234	066	76 SE	6 of 7	9.09	43320	28	478	1909	1.7	2.3	39.3	−25.7	9.0	N
							AREA B									
200454	G	3958	-	-	3 of 3	0.31	9351	20	423	92	12.9	10.1	159.5	51.1	46.5*	U
200830	G	3708	-	-	4 of 5	0.07	4146	5	471	42	14.3	16.1	220.3	45.5	21.9*	R
200910	G	3672	-	-	3 of 4	0.33	2436	29	522	572	5.2	3.1	27.4	−28.0	4.0	N
201052	G	3627	-	-	4 of 4	0.30	5315	34	536	231	6.1	5.6	71.6	−21.7	37.8	N
210228	D	3136	045	66 SE	4 of 4	0.86	11419	52	230	81	10.3	9.0	110.1	28.4	86.6*	U
210411	D	3037	056	46 SE	2 of 2	2.66	31590	76	320	242	16.1	5.2	30.4	−11.2	13.9	N
220248	G	3942	-	-	3 of 3	2.21	26779	10	541	244	7.9	3.8	211.9	−43.3	68.4*	U
220259	D	3937	-	-	3 of 3	1.72	24664	15	545	499	5.5	4.0	223.8	−55.0	80.9*	U
220333	D	3884	-	-	3 of 3	1.51	20710	43	536	227	8.2	5.4	254.1	−48.2	83.1*	U
220350	D	3876	-	-	3 of 3	26.55	31462	24	541	136	10.6	7.0	211.5	−49.3	74.4	U
220852	D	3197	049	58 SE	2 of 2	3.34	26990	19	-	398	12.5	4.0	280.0	−61.0	77.4	U
220941	D	3142	086	61 SE	2 of 2	4.38	44664	15	556	1191	7.2	2.3	37.9	−22.1	7.5	N
221200	D	2930	092	63 SW	3 of 3	6.16	29456	21	554	61	11.8	10.3	40.7	−13.5	15.1	N
222213	D	3163	065	51 SE	3 of 4	2.99	33282	22	559	847	4.2	3.0	355.5	−42.8	33.6	N
230509	D	2979	081	67 SE	5 of 5	11.53	49638	15	558	885	2.6	2.8	215.3	0.4	25.1*	R
811921	D	3174	051	76 SE	4 of 4	11.63	20260	14	552	88	9.9	8.6	13.3	−19.9	16.6	N
811933	D	3147	044	85 SE	2 of 2	12.26	30662	26	554	2103	5.4	1.8	39.9	−12.5	15.5	N
811947	D	3119	042	71 SE	6 of 6	7.46	26954	21	556	185	4.9	6.0	2.1	−8.3	31.8	N
812005	D	3117	045	78 SE	2 of 2	2.78	29519	24	531	1151	7.4	2.4	41.0	−28.4	10.0	N
812019	D	3114	062	62 SE	6 of 6	15.63	48256	13	546	2589	1.3	1.6	54.4	−32.6	22.3	N
812035	D	3114	012	84 SE	3 of 3	5.31	46370	23	509	312	7.0	4.6	24.6	−28.5	6.2	N
812047	D	3113	048	67 SE	5 of 5	4.42	-	26	-	392	3.9	4.1	32.5	−23.6	2.4	N
812110	D	3088	066	55 SE	6 of 6	7.32	58562	12	559	796	2.4	2.9	17.0	−46.1	23.6	N
812124	D	3083	048	79 SE	5 of 5	5.00	51241	13	530	526	3.3	3.5	29.9	−24.2	1.0	N
812132	D	3083	050	73 SE	5 of 6	2.86	38470	19	541	185	5.6	6.0	32.4	−21.1	4.4	N
812149	D	3081	049	79 SE	5 of 5	9.15	43624	11	553	1151	2.3	2.4	32.8	−41.7	16.7	N
812209	D	3035	048	64 SE	5 of 5	3.43	28381	17	556	588	3.2	3.3	26.7	−36.9	12.2	N
812234	D	2985	044	68 SE	4 of 4	4.44	57488	14	554	513	4.1	3.6	53.3	−26.8	20.6	N
812248	D	2968	056	70 SE	6 of 6	2.47	40275	12	557	177	5.0	6.1	14.4	−10.0	21.4	N
821651	D	3093	054	67 SE	3 of 3	17.97	62198	15	557	522	5.4	3.5	18.6	−39.4	17.4	N
822002	D	2942	058	73 SE	5 of 5	5.00	38383	12	556	710	2.9	3.0	12.6	−28.0	16.2	N
831644	D	3075	036	75 SE	3 of 3	0.28	18828	61	-	126	11.0	7.2	12.6	70.9	83.2*	U
831706	D	3062	232	74 NW	3 of 3	9.48	61067	40	-	108	11.9	7.8	127.1	−30.5	82.9	U
831750	D	3018	054	69 SE	6 of 6	2.72	15483	85	276	87	7.2	8.7	53.3	−13.4	24.5	N
831829	D	2937	156	61 SW	3 of 3	5.31	26519	76	278	1938	2.8	1.8	31.8	−34.8	9.8	N
831917	D	2849	048	64 SE	2 of 2	1.99	25867	62	476	1017	3.9	2.5	19.2	−30.4	11.2	N
831937	D	2839	026	83 SE	2 of 2	1.36	36343	19	-	899	8.3	2.7	42.3	78.7	76*	U
841759	D	2908	022	61 SE	2 of 2	10.20	38557	40	476	2025	2.7	1.8	358.0	−50.3	35.4	N
841830	D	2768	055	64 SE	3 of 3	13.55	29789	39	532	278	5.5	4.9	32.9	−3.0	22.2	N
861711	D	3095	070	58 SE	3 of 3	7.36	36165	22	551	6516	1.5	1.0	45.5	13.8	41.6	N
861740	D	3073	070	64 SE	2 of 2	22.41	42132	22	-	1180	7.3	2.4	20.7	9.4	35.8	N

Table 1. (continued)

Sample	Rock Type[b]	Depth (m)	Attitude[c] Strike (deg)	Attitude[c] Dip (deg)	N/Nc	NRM (A/m)	X, (μSI)	Stability[d] MDF′, (mT)	Stability[d] MDT′, (°C)	k	α95 (deg)	csd (deg)	D (deg)	I (deg)	Angle (deg)	Pol[e]
861843	D	2977	053	69 SE	7 of 7	5.84	27667	38	538	73	7.1	9.5	43.6	−21.9	12.5	N
861905	D	2893	062	64 SE	5 of 5	7.46	42987	45	515	611	3.1	3.3	44.5	−19.2	14.3	N
861925	D	2823	069	61 SE	4 of 4	5.98	31520	23	349	1464	2.4	2.1	17.5	−19.9	13.0	N

[a]Sample numbers are combination of truncated dive number and dive times. NRM is natural remanent magnetization at room temperature; N/N_c is number of cores measured (N) versus number used in final sample mean calculation; D and I are declination and inclination, respectively.
[b]Sample lithology: dike (D) or gabbro (G).
[c]Orientation of dike chilled margin from Geocompass measurements.
[d]MDF′ is median destructive field (mT), at which 50% of initial NRM remains; MDT′ is median destructive temperature (°C), at which 50% of initial NRM remains; Angle is the angle between the sample remanence direction and calculated bootstrap mean direction or its antipode (marked with asterisk *) for normal or reverse polarity, respectively.
[e]Sample polarity interpretation: normal (N), reverse (R), or undetermined (U).

demagnetization levels. In the case of AF experiments, specimens were subjected to stepwise-increasing fields in 2.5 mT steps to 20 mT, 5 mT steps between 20 and 30 mT, and 10 mT steps between 30 mT and 100 mT. In thermal demagnetization experiments, temperature was raised in 50°C steps from 100°C to 500°C and in 25°C steps between 500°C and 600°C. More detailed thermal demagnetization steps of 10°C were implemented between 500° and 570° with two subsequent 5°C steps up to 580°C for some gabbroic specimens. All magnetization components were determined by principal component analysis [*Kirschvink*, 1980]. The average direction for each block sample was calculated from the characteristic remanent magnetization (ChRM) directions of specimens based on Fisher statistics [*Fisher*, 1953].

[19] To calculate mean directions and uncertainties at the site-level (e.g., dive transect or area) requires a non-Fisherian statistical analysis, due to inclusion of potentially misoriented sample remanence directions whose overall distribution would not pass the Fisher assumptions. Rather than arbitrarily rejecting individual sample remanence directions, we choose to use a statistical bootstrap [*Tauxe et al.*, 1991], or resampling, technique to calculate mean directions and their uncertainties from samples collected in Area A and Area B. One intrinsic benefit of the bootstrap method is that it assumes that all uncertainty inherent in the data is reflected in the distribution; this provides an estimate of the potential uncertainties related to seafloor sampling and subsequent reorientation methods. If there are a large number of misoriented blocks, then the bootstrap method would result in large uncertainties that should be more representative of the true uncertainties related to the seafloor sampling methods.

[20] Previous studies use an estimated additional 10° uncertainty to account for increased scatter related to the sampling procedure [*Varga et al.*, 2004]. However, detailed sample collection from a series of adjacent dikes during *Alvin* Dive 4081 allows identification of gross misorientations and provides confidence in the technique where only a single or a few blocks are collected in a small area. The uncertainties calculated for this particular dive sample set appear relatively low and represent our best attempt to average secular variation, although the nominal time represented by the ~200 m lateral coverage during this dive is ~3 ka, assuming a half-spreading rate of 71 mm yr^{-1}. The exact time required to average out geomagnetic secular variation is not well known, but typical estimates are 10^4–10^5 years [*Tauxe*, 2010]. Due to the relatively few oriented samples collected during most transects within coherent structural blocks and the necessity to average over a longer amount of time, we chose to bootstrap block sample remanence directions separately in each area. Each area represents ~55 ka of spreading across 4 km parallel to the spreading direction, and the combination of the two domains represents ~110 ka of spreading across 8 km, assuming a half-spreading rate of 71 mm yr^{-1}.

5. Results

[21] Paleomagnetic remanence of 62 fully oriented dike and 5 gabbro block samples are discussed below and summarized in Table 1. More detailed descriptions of collection sites and their geologic context can be found elsewhere [*Karson et al.*, 2005; J. A. Karson et al., unpublished cruise report, 2005; Chutas, unpublished thesis, 2007], and on the *Alvin* Frame Grabber (http://4dgeo.whoi.edu/alvin) and *Jason II* Virtual Van (http://4dgeo.whoi.edu/jason) websites.

5.1. Magnetic Remanence Results

[22] The natural remanent magnetization (NRM) intensities of the dikes from Pito Deep Rift range from 0.07 to 26.6 A/m (Table 1). The large collection of specimens derived from 62 dike blocks reveals that the magnetization intensities are approximately lognormally distributed (Figure 8), with an arithmetic mean of 5.96 A/m ± 3.76 and a geometric mean of 4.28 A/m.

[23] The majority of dike specimens from Pito Deep exhibit nearly univectorial demagnetization behavior (Figure 9). Minor lower stability overprints are rarely present, and are typically removed at temperatures of 250–300°C or 10–15 mT. A maximum blocking temperature determined by thermal demagnetization is typically ~575°C (Figure 9), suggesting that remanence in most samples is primarily carried by nearly pure magnetite, or very low-Ti titanomagnetite. The median destructive field (MDF′), or the alternating field that reduces the vector difference sum of the remanence to half its initial value, was calculated to measure specimen stability to alternating fields. In an anal-

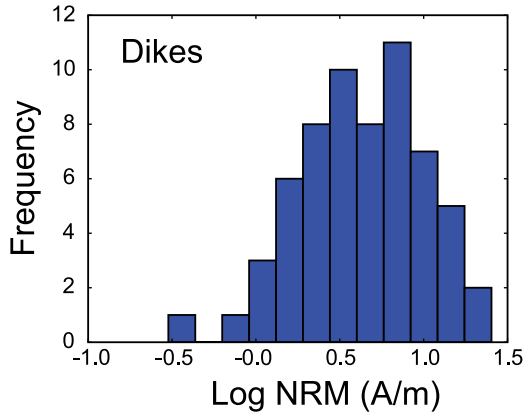

Figure 8. Log of natural remanent magnetization (NRM) of 62 dike blocks from Pito Deep Rift. Arithmetic mean = 5.96 A/m ± 3.76; geometric mean = 4.28 A/m.

ogous manner, the median destructive temperature (MDT′) was calculated for thermally demagnetized specimens. The Pito Deep dike samples typically have moderate stability, with a mean MDF′ of 26 mT and a mean MDT′ of 499°C. All samples have MDF′ values of ≥5 mT.

[24] NRM intensities of five gabbroic blocks from the Pito Deep Rift area range from 0.21 to 2.21 A/m (Table 1). The arithmetic mean of 0.67 A/m ± 0.62 and a geometric mean of 0.42 A/m. These samples typically have moderate stability, with mean MDF′ = 20 mT; mean MDT′ = 498°C. Detailed thermal demagnetization of the gabbro specimens in a shielded paleomagnetic lab reveal the presence of samples with one, two, or three-component remanence (Figure 9, k, l, m). Although cooling through polarity intervals is not unexpected since the study areas are both located near reversal boundaries, we have insufficient data to draw any conclusions.

5.2. Paleomagnetic Remanence Directional Results

[25] Remanence directions from all 67 oriented samples yield demagnetization data that are fairly well-grouped (Figures 10 and 11 and Table 1). Results from nearly every specimen allow a single, high-stability-component remanence direction to be isolated, although the quality of the results varies. The specimen ChRM directions are typically well-defined, with an average maximum angle of deviation (MAD) of 1.7°. Sample average directions are well determined; 85% have $\alpha_{95} < 10°$, and CSD values (which do not depend on number of samples (n)) are typically also < 10° (Table 1). No results are rejected from the statistical analysis.

[26] During *Alvin* Dive 4081, a set of fourteen block samples of adjacent dikes was collected along the spreading direction within one coherent crustal block (site) to test the consistency of the paleomagnetic data by assessing scatter related to sampling procedure. At the site level (dive transect), sample mean vector (SMV) remanence directions appear well clustered (Figure 12), and a statistical bootstrap of the SMV was used to calculate the mean direction and confidence limits for the Dive 4081 subset. The mean direction (D = 029.4° ± 9.6°, I = −26.5° ± 6.2°) plots well away from the Geocentric Axial Dipole expected direction (GAD; D = 000°, I = −40.2°) at the 95% confidence level (Figure 12). Uncertainties calculated for this particular dive sample set appear relatively low. Unfortunately, data sets with less than about 25 elements produce bootstrapped confidence regions that are in general too small [*Tauxe et al.*, 1991]. Although the data need not be Fisherian, they can be plotted against an expected value for a specific distribution in a quantile-quantile plot [*Fisher et al.*, 1987]. These directional data pass the test for a Fisherian distribution on a quantile-quantile plot with values of $M_u = 0.764$ and $M_e = 0.744$, well below the critical values of 1.207 and 1.094, respectively [*Fisher et al.*, 1987; *Tauxe*, 2010]. The data from Dive 4081 are Fisherian and give an α_{95} of 8.8° on the mean direction, that suggests this group of dike samples is from an intact unit.

[27] A majority of the remanence directions from 62 dike and 5 gabbro samples show declinations to the northeast with moderate to shallow negative inclinations (Figure 13), as would be predicted for ~3 Ma crust produced during a dominant normal polarity at ~23° S. Although few directions appear widely scattered, the bulk of the directions are similar to those from *Alvin* Dive 4081 (Figures 12 and 13). Directions of the highest stability component from the five gabbro samples are also distinct from the expected GAD direction at the 95% level of confidence, although considerable scatter is observed (Figure 13). Similar to the example from Dive 4081, a statistical bootstrap technique is used to calculate mean directions and 95% confidence limits of SMV from 23 fully oriented samples in Area A (D = 38.9° ± 8.1°, I = −16.7° ± 15.6°), and 44 samples in Area B (D = 31.4° ± 7.5°, I − 26.6° ± 8.4°, n = 34; D = 203.1° ± 39.6°, I = 14.1° ± 72.4°, n = 10) (Figure 13). Area B yields a negative inclination (normal polarity) and a positive inclination (reverse polarity) mode. The overall bootstrapped mean for Area B after inverting reverse polarity directions is D = 30.4° ± 8.0°, I = −25.1° ± 12.9° n = 44. The 95% confidence bounds of the two bootstrapped mean directions overlap; however, since neither confidence limit includes the mean direction of the other, an additional test is needed. A bootstrap test for a common mean direction [*Tauxe et al.*, 1991], between the two data sets found overlapping 95% confidence bounds for all three Cartesian coordinate components, which indicates that the two bootstrapped means for Area A and B are not distinguishable at the 95% confidence level. A similar test demonstrates that both overall bootstrapped mean directions from each area are distinct from the GAD expected direction at the 95% confidence level (Figure 13). This distinction suggests significant, post-emplacement structural rotations. To evaluate potential rotation axes, we rely heavily on geologic and structural observations and consistent, accurate Geocompass measurements of dike orientations.

6. Sampling Orientation Uncertainties and Interpretation

[28] Undoubtedly, methods of submersible collection of blocks and subaerial sample reorientation procedure provide numerous potential sources of uncertainties in the site mean remanence directions. Several steps were added to the procedure at Pito Deep Rift in response to experience gained during the Hess Deep Rift cruise to greatly reduce orientation errors at all stages of collection and handling of block

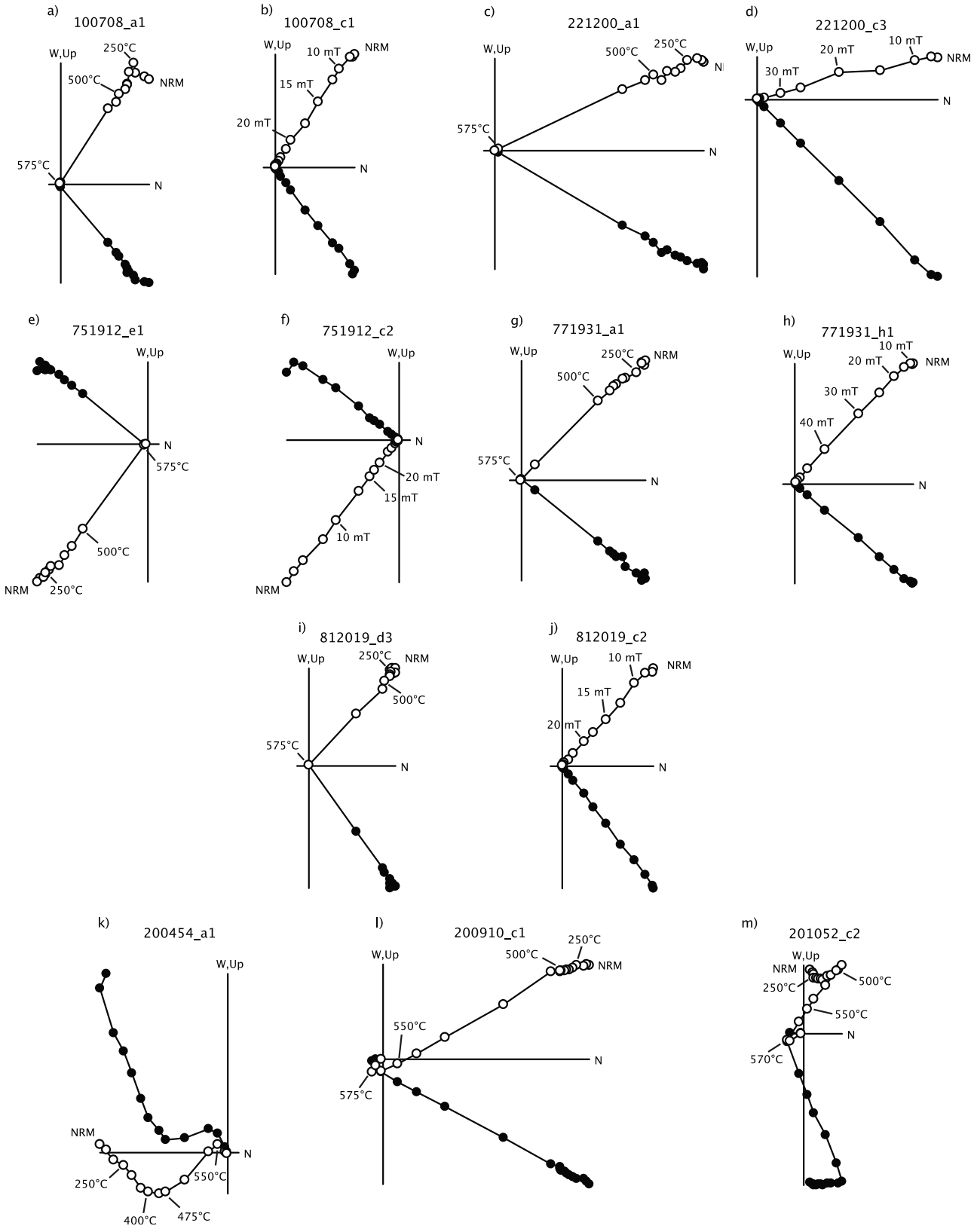

Figure 9. Vector endpoint diagrams show thermal and alternating field demagnetization behavior from representative specimens from Pito Deep Rift dike and gabbro samples. Filled (open) circles are the horizontal (vertical) projections. Diagrams a–j show specimens from basalt dikes. Diagrams k–m show specimens from gabbros with two and three component remanence directions.

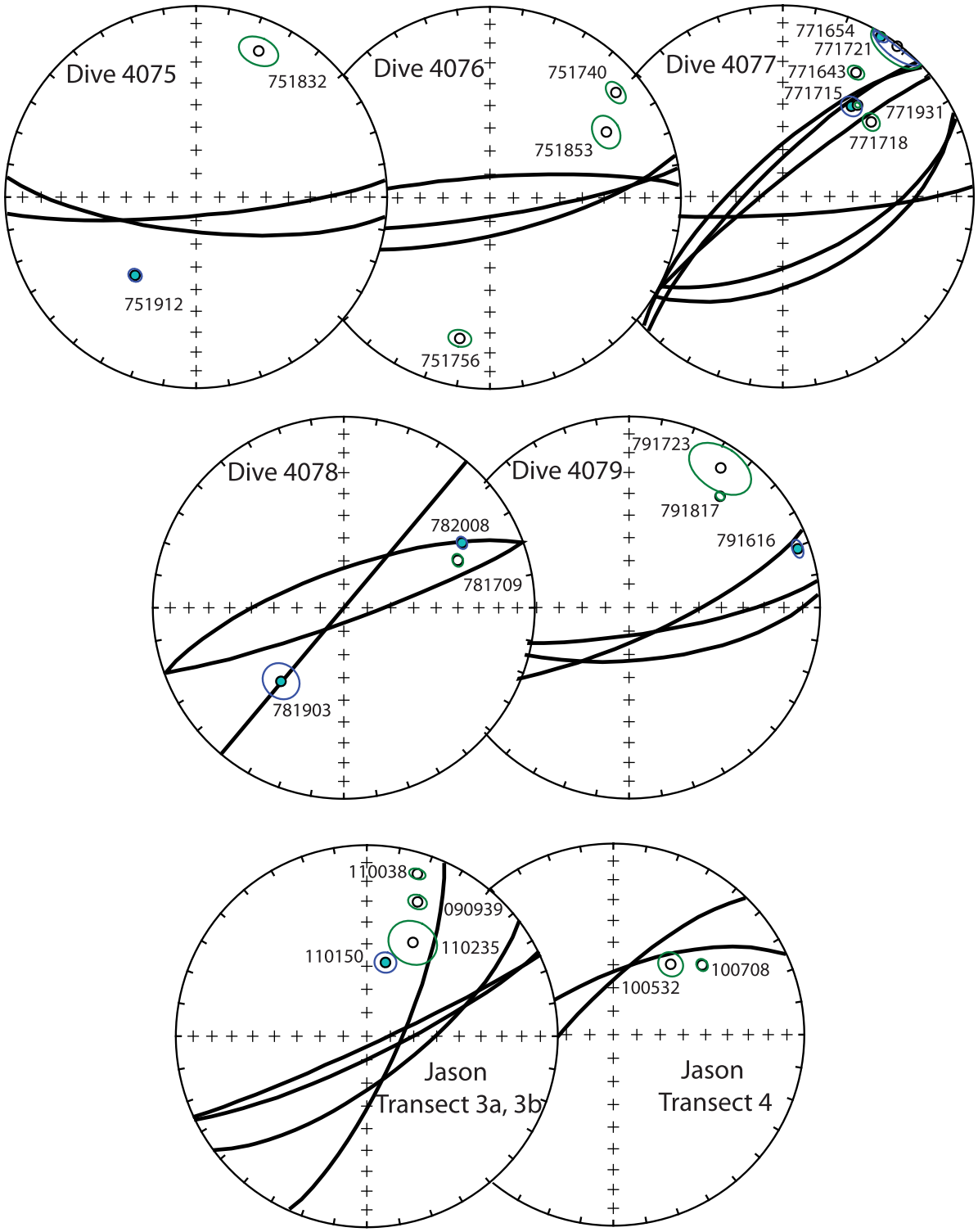

Figure 10. Lower-hemisphere, equal-area stereonets showing sample mean vector (SMV) directions from Area A in Pito Deep Rift. Open (filled) symbols are for the upper (lower) hemisphere, and small circles are $\alpha 95$ confidence ellipses. Great circles represent dike orientations measured on samples at every collection site during each dive.

samples. The careful shipboard procedure eliminated the most obvious errors related to in situ block orientation measurements, however, we suspect that some uncertainty related to seafloor sampling or during later reorientation remains. Approximately 14 out of 67 block samples yielded stable remanence directions that strongly diverge from other adjacent blocks collected during the same individual dive transect and cannot be readily interpreted in terms of

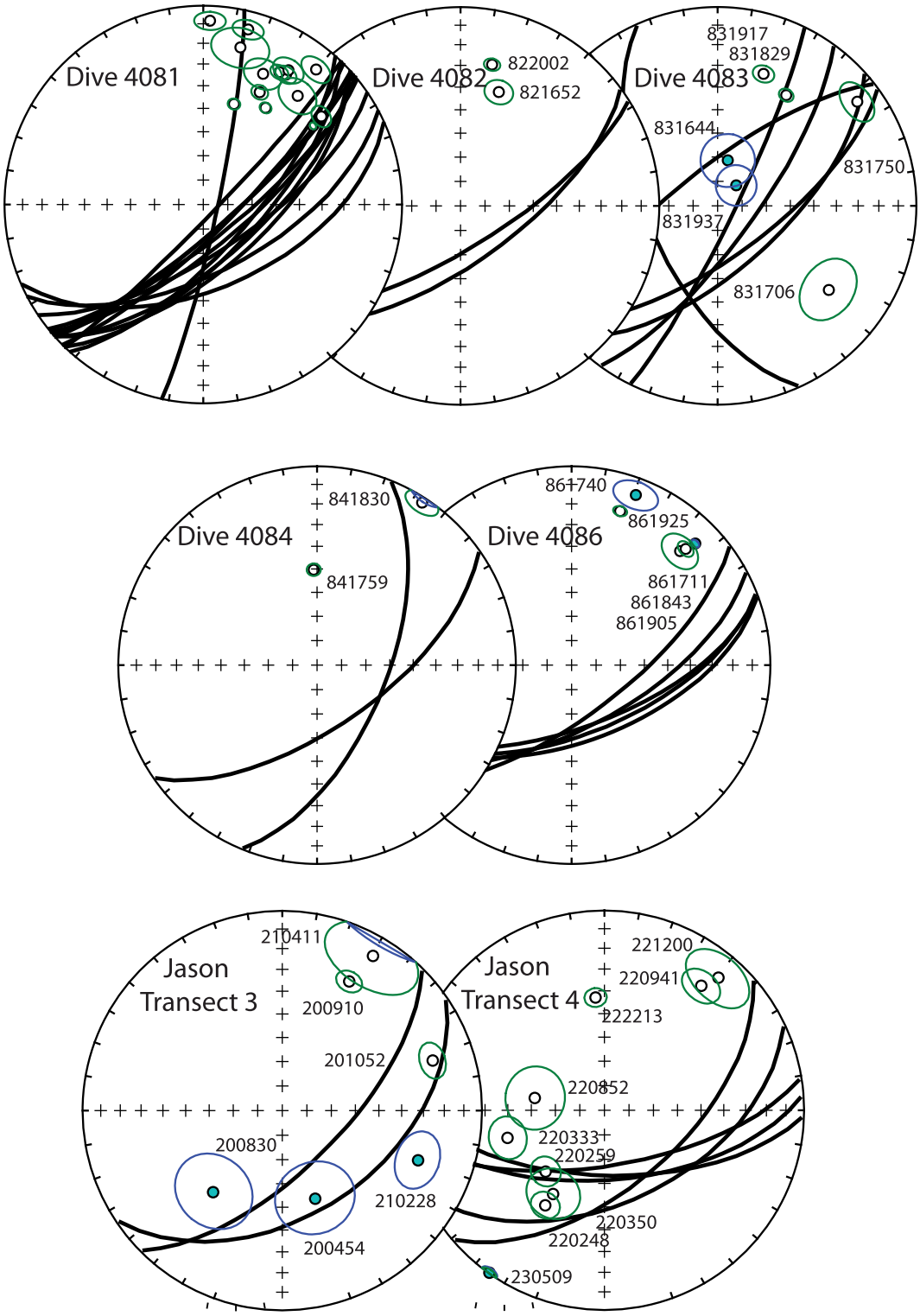

Figure 11. Lower-hemisphere, equal-area stereonets showing sample mean vector (SMV) directions from Area B in Pito Deep Rift. Symbols same as in Figure 10.

polarity or explained with any reasonable rotation history for which there is geologic evidence.

[29] A number of factors potentially lead to scatter of paleomagnetic directional data. These include (1) uncertainty in block orientation during initial seafloor sample collection, (2) uncertainty during later, post-cruise block reorientation, (3) uncertainty in the measurement caused by instrument noise or sample alignment errors, (4) geomagnetic secular variation, and (5) variable tectonic rotations. As mentioned above, great effort was made to reduce some of these errors (e.g., 1 and 2). Few of these sources of error lead to symmetric distributions about a mean direction

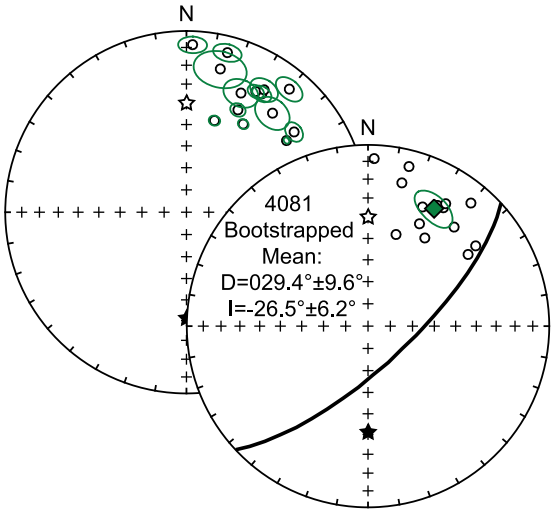

Figure 12. Equal-area stereonet of sample mean vector (SMV) directions and corresponding α_{95} confidence ellipses for all 14 adjacent dike samples collected during Alvin Dive 4081. Open circles plotted in upper hemisphere. Open (filled) star represents expected direction for normal (reversed) geocentric axial dipole at ~23° S. Also shown in the accompanying stereonet is the bootstrapped mean of these 14 dikes with estimated 95% confidence ellipse. This mean direction is distinct from the expected direction at this level of confidence, suggesting some rotations have occurred. Great circle depicts average dike orientation measured for 14 samples, 047°/72° SE.

(e.g., 3), and these uncertainties at the sample (block) level contribute to the value of the α_{95} confidence ellipse. Scatter related to geomagnetic and geologic sources (e.g., 4 and 5, respectively) affect the scatter of remanence directions and can be assessed by calculating bootstrap mean directions from multiple SMV in each study area.

6.1. Polarity Interpretation

[30] The two focused survey areas span normal polarity Chron C2An.2n and Chron C2An.3n in Areas A and B, respectively (Figure 2). Due to the proximity of the study areas to polarity transition zones, it is possible that some samples record reverse polarity intervals or transitions near the northwestern and southeastern flanks of either Area A or B. Polarity interpretations are determined from the proximity of SMV directions to the bootstrapped mean direction or its antipode, evaluated with a cutoff angle of 44° (Table 1). The angle 44° is the minimum solid angle between the bootstrapped mean direction and a set of fictitious sample directions generated from simulations of various combinations of potential 90° misorientations of block samples (i.e., wrong surface noted, etc.). SMV within 44° to the bootstrapped mean or its antipode in each area are labeled normal (N) or reverse (R), respectively. Samples that yield directions greater than 44° to the bootstrapped mean or antipode are labeled as undetermined (U), and are typically very different than other SMV directions collected on the same dive. These 14 SMV are difficult to interpret in terms of polarity because they could reflect transitional directions or grossly misoriented samples (Figure 14 and Table 1).

[31] Dominant normal polarity of Pito Deep Rift paleomagnetic data (Table 1) is consistent with crustal generation during the two normal polarity Chrons, Chron C2An.2n (3.110–3.220 Ma) and Chron C2An.3n (3.330–3.580 Ma) [*Cande and Kent*, 1995]. Very few SMV directions interpreted as reverse polarity suggest that a few dikes were either injected into a normal polarity section of sheeted dikes during a subsequent reverse polarity interval, or perhaps the opposite scenario in which several dikes injected into panels of reverse polarity sheeted dikes during a subsequent normal polarity (Figure 14). Assuming dike intrusion occurs in a very narrow (few 100 m) zone at fast- to superfast spreading ridges [*Hooft et al.*, 1996], the polarity transition within the sheeted dike complex should occur across a similar width. However, in Area A, two reverse polarity dike samples were collected during two *Alvin* Dive transects that are ~1.5 km apart (4075 and 4078). Although only represented by two samples, these suggest that the active zone of intrusion may be significantly wider than a few hundred meters, or that dikes may be intruded ≥1 km off-axis.

[32] The gabbro samples collected from Area B provide some indication of the thermal structure and tectonic history of Pito Deep Rift. Several gabbro specimens exhibit a range in demagnetization behavior from nearly univectoral remanence to multicomponent remanent magnetization with up to three components (Figure 9). In a few specimens the highest stability component is interpreted as reverse polarity with a moderate to lower stability component of inferred normal polarity. This suggests that some of these gabbroic rocks cooled during a reverse to normal polarity transition likely represented by Chron C2An.2r to C2An.2n (3.220–3.330 to 3.220–3.110 Ma). Two gabbro blocks are interpreted as undetermined polarity. A similar range in directional variability was observed in Hess Deep Rift gabbros [*Varga et al.*, 2004].

6.2. Structural Rotation Models

[33] Geologic relationships and magnetic remanence directions provide constraints and guidance to any rotation models. The geometry and timing of rotations is constrained by the geology and tectonic history of the area, and any interpretation relies on several important assumptions. The main assumption in the use of paleomagnetic directional data to document structural rotations is that remanence was acquired over sufficient time to average secular variation so that the initial remanence direction coincides with the time-averaged geocentric axial dipole (GAD) direction at the site latitude. Similar to other paleomagnetic studies of sheeted dikes [e.g., *Allerton and Vine*, 1987], additional assumptions include the following: (1) observed stable remanence directions predate structural rotations, (2) initial dike orientations are near vertical and ridge-parallel, and (3) little internal deformation of each dike results in a constant angle between the remanence vector and the pole to the dike during deformation.

[34] As suggested from early paleomagnetic studies of sheeted dikes in the Troodos Ophiolite, a single, unique rotation could account for the discrepancy between the observed remanence directions and the expected direction [*Allerton and Vine*, 1987]. However, this arbitrary single-rotation approach is not realistic in areas with more than one structural event or period of deformation. For example,

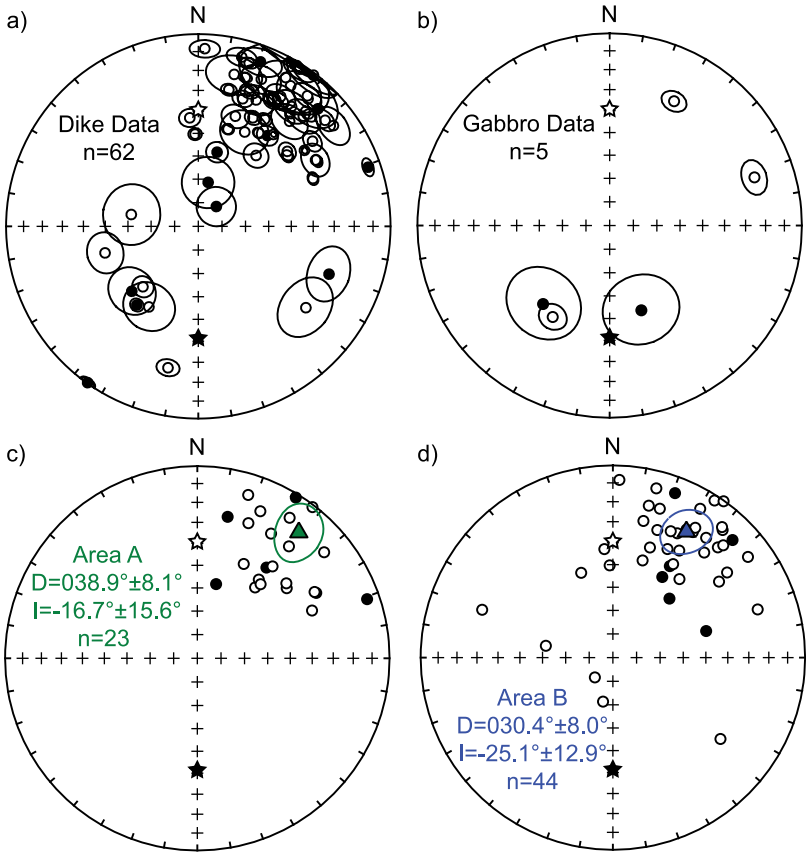

Figure 13. (a) Equal-area stereonet of sample mean vector (SMV) directions and corresponding α_{95} confidence ellipses for all 62 dike samples collected during from Pito Deep Rift. Open (filled) circles plotted in upper (lower) hemisphere. Open (filled) star represents geocentric axial dipole expected direction at ~23° S for normal (reversed) polarity. (b) Data from all 5 gabbro samples with same symbols. (c) Bootstrapped mean for all samples in Area A (23), with antipodes of reversed polarity samples (Table 1). (d) Bootstrapped mean for all samples in Area B (44), with antipodes of reversed polarity samples (Table 1). Bootstrapped mean remanence directions from both Areas are distinct from the expected direction at this level of confidence, suggesting some rotations have occurred.

remanence directions from dikes in Troodos can alternatively be restored using a sequence of rotations constrained by the geologic history of the ophiolite [*Varga et al.*, 1999]. Similarly, a single rotation solution is not geologically plausible in the case of sheeted dikes exposed at Pito Deep Rift, as it likely averages over distinct structural events that give rise to the net rotational history. Instead, several geological observations provide a framework to guide interpretation and development of the following models of the structural rotation history of uppermost crust exposed at Pito Deep Rift.

[35] At least three possible rotations are likely to have affected the uppermost crust exposed on the northeastern wall of the Pito Deep Rift [*Handschumacher et al.*, 1981; *Searle et al.*, 1989; *Martinez et al.*, 1991; *Naar et al.*, 1991]. A first possible rotation about an approximately north-south (EPR-parallel) horizontal axis may be related to subaxial subsidence processes as suggested from other studies of fast-spread uppermost crustal structure and generally observed outward dip of the sheeted dikes [*Karson*, 2002; *Varga et al.*, 2004, 2008]. The trend of this EPR-parallel rotation axis could vary from ~004° to ~016° as observed from current EPR-axial trends between 20° to 23° S latitudes [*Naar and Hey*, 1991]. Tectonic reconstructions depict similar NNE trends of the EPR axis of 010° and 015° at ~3.5 and 3.0 Ma, respectively [*Rusby and Searle*, 1995]. The magnitude of this ridge-axis rotation is possibly equal to the plunge of the average dike poles, 6.6° ± 9.3° (or 15.1° ± 9.7° for 2/3 majority of dikes) and 22.5° ± 6.5° in Area A and B, respectively. In order to evaluate initial spreading-related rotations, it is necessary to remove the effects of other subsequent rotations. A second possible rotation is approximated by a vertical-axis rotation related to the clockwise rotation of the Easter Microplate. Based on abyssal hill and magnetic anomaly lineaments that deviate from EPR-parallel to the north of Pito Deep, the vertical-axis rotation magnitude is thought to be 20°–55° clockwise [*Naar and Hey*, 1991; *Naar et al.*, 1991]. The abyssal hill lineaments across the blocks in Area A and B trend ~065°, and ~057°, respectively (Figure 2); both of these trends are essentially parallel to the average strike of dikes in each area within the uncertainties (65.6° ± 9.3° for all, or 68.6° ± 9.7° for 2/3 majority in Area A; and 54.3° ± 6.5° in Area B). A third possible rotation is a horizontal-axis rotation about

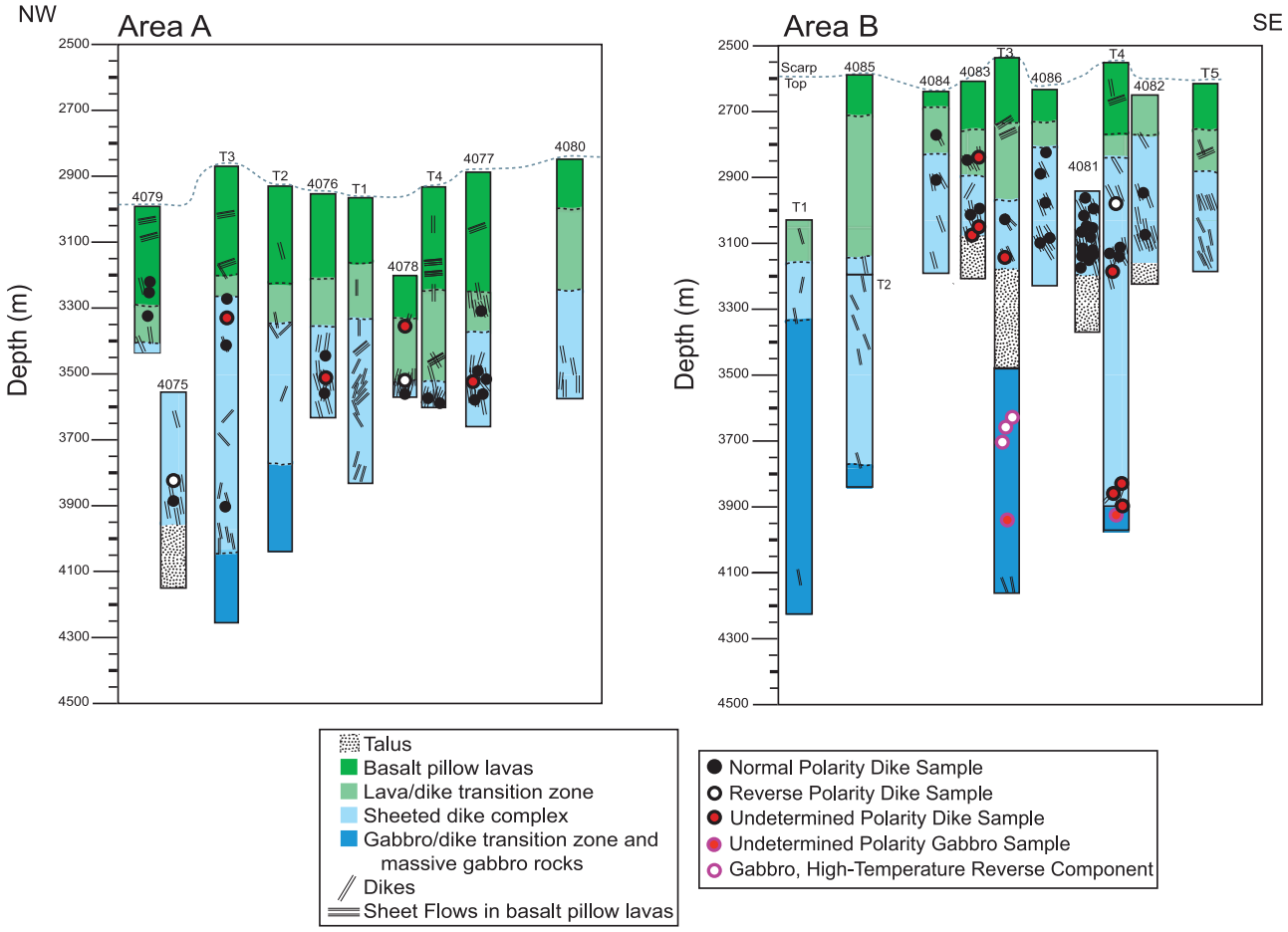

Figure 14. Spatial relationship of polarity interpretation of samples collected by *Alvin* and *Jason II* shown on lithologic columns of individual transects in both study Areas at Pito Deep Rift (after Chutas, unpublished thesis, 2007).

Table 2. Comparison of Paleomagnetic Bootstrapped Means and Rotational Models

Model Stage	Rotation Description	Rotation Axis	Amount	Mode	Bootstrapped Mean n	Bootstrapped Mean Declination	Bootstrapped Mean Inclination
			Area A				
	No rotation	-	-	1	3	-	-
	No rotation	-	-	2	20	40.3° ± 8.7°	−15.8° ± 16.0°
	No rotation	-	-	Combined	23	38.9° ± 8.1°	−17.0° ± 15.6°
1	Block tilting of Pito Deep Rift	330°/00°	−25°	Combined	23	33.2° ± 8.1°	−39.8° ± 15.6°
2	Easter microplate rotation	000°/90°	−33°	Combined	23	000.3° ± 8.1°	−39.8° ± 15.6°
1	Block tilting of Pito Deep Rift	330°/00°	−21°	Combined	23	34.7° ± 8.1°	−36.1° ± 15.6°
2	Easter microplate rotation	000°/90°	−46°	Combined	23	348.7° ± 8.1°	−36.2° ± 15.6°
3	Subsidence accommodation at EPR axis	010°/00°	11°	Combined	23	357.0° ± 8.1°	−39.5° ± 15.6°
			Area B				
	No rotation	-	-	1	10	203.4° ± 40.1°	13.8° ± 90.0°
	No rotation	-	-	2	34	31.4° ± 7.5°	−26.7° ± 8.4°
	No rotation	-	-	Combined	44	30.3° ± 8.0°	−25.1° ± 12.8°
1	Block tilting of Pito Deep Rift	330°/00°	−18°	Combined	44	24.1° ± 8.0°	−40.2° ± 12.8°
2	Easter microplate rotation	000°/90°	−24°	Combined	44	000.1° ± 8.0°	−40.2° ± 12.8°
1	Block tilting of Pito Deep Rift	330°/00°	−10°	Combined	44	27.5° ± 8.0°	−33.6° ± 12.8°
2	Easter microplate rotation	000°/90°	−44°	Combined	44	343.5° ± 8.0°	−33.6° ± 12.8°
3	Subsidence accommodation at EPR axis	010°/00°	22°	Combined	44	359.7° ± 8.0°	−40.6° ± 12.8°

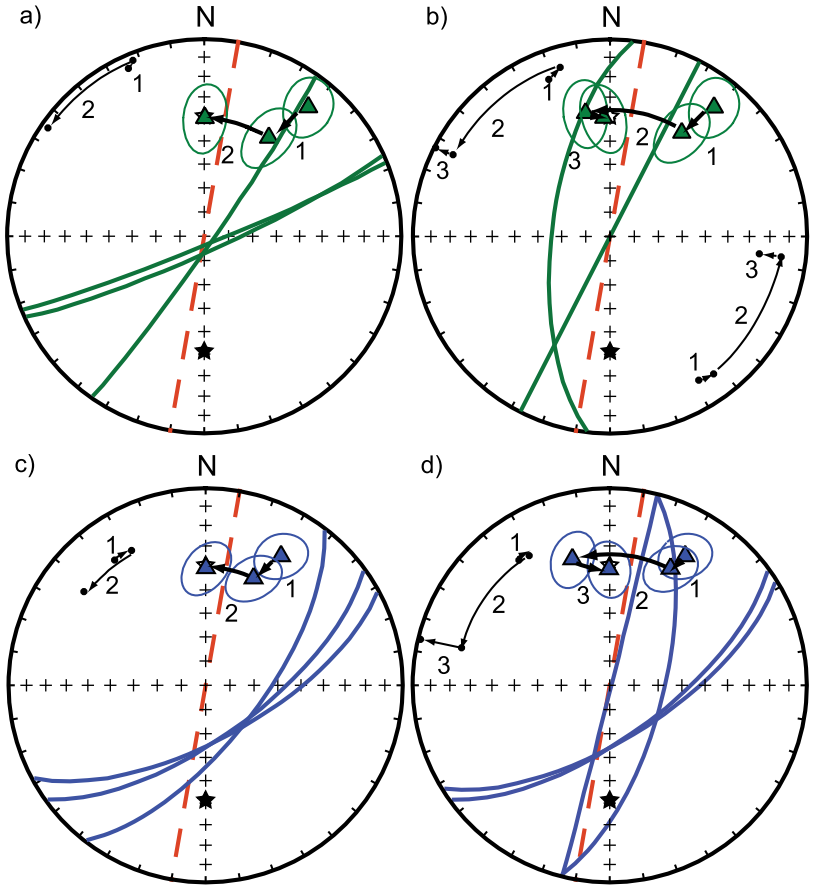

Figure 15. Equal-area stereonet illustrations of rotation models for Areas (a and b) A and (c and d) B. The bootstrapped mean remanence directions of the samples are shown by the triangle with its corresponding α_{95} confidence ellipse. Open (filled) star represents geocentric axial dipole expected direction at ~23° S for normal (reversed) polarity. Dashed red great circle shows expected dike orientation (010°/90°), parallel to the EPR axis and vertical. Great circles and their poles correspond to the average dike orientations in each Area and track changes in orientation throughout the rotation sequence. However, only the two final restored orientations of the two sets of dikes in Area A are shown in Figure 15b for clarity. These stereonets show the two-stage (Figures 15a and 15c) and three-stage (Figures 15b and 15d) reverse sequence of different rotations outlined in the text and Table 2. Numbers represent reverse sequence of rotations: 1, Pito Deep Rift block tilting rotation about 330°/00° horizontal axis; 2, Easter Microplate vertical-axis (000°/90°) rotation; and 3, EPR axis (010°/00°) horizontal axis. See section 6.2 and Table 2 for further description and magnitude for each rotation.

an axis parallel to the trend of the Pito Deep Rift (~330°) related to rifting [*Martinez et al.*, 1991]. Unfortunately, constraints on the magnitude of northeastward tilting such as the dips of lava flows high in the crustal section or bedding in overlying sedimentary rocks have not been determined in either study area. However, the gentle east-facing bathymetric slope of the shallow, large-scale (10–15 km) coherent crustal blocks east of Pito Deep noted by *Martinez at al.* [1991], suggest that these blocks were tilted ~10° or more to the NE during rifting.

[36] Although any number of structural rotations can account for the orientation of dikes and observed remanence directions, the rotation axes and approximate magnitudes outlined above represent a likely sequence of geologic events for the study areas. No amount of rotation about one of these single axes alone restores the remanence direction, so at least two of these proposed rotations must have occurred. We can create a series of rotation models based on the geologic relationships outlined above using 1° incremental amounts of rotation along these paths by using a similar strategy for restoration of remanence directions as *Varga et al.* [1999], and remove rotations in reverse order of formation (the most recent rotation affecting the remanence directions should be removed first followed by older rotations, in a reverse sequential order). If we assume secular variation has been successfully averaged, then the initial, expected remanence direction should be near the GAD direction (000°/−40.2°). We can constrain the rotation models by using the uncertainty of the bootstrapped mean directions from Area A and B and the amounts of rotation about the specified axes that restore the confidence ellipse to include the expected GAD direction. In this way, we can constrain

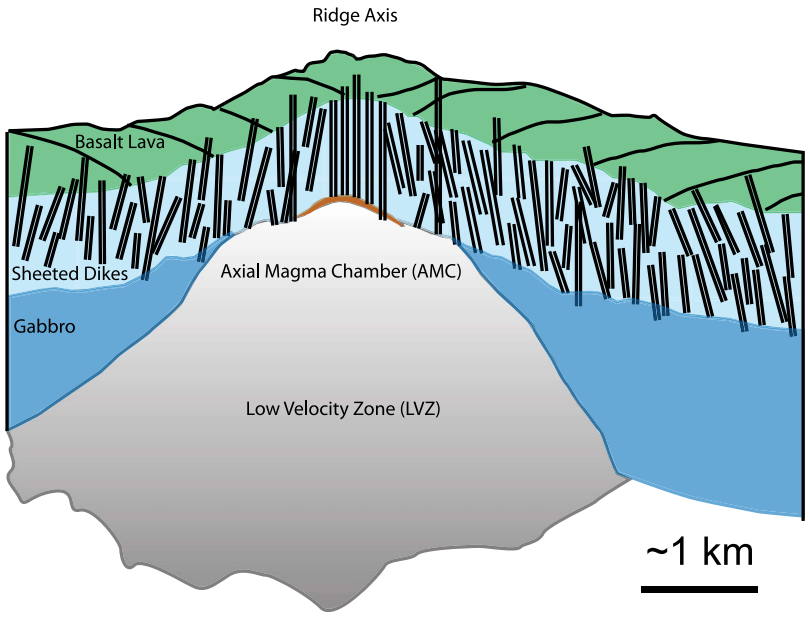

Figure 16. Schematic diagram of superfast spreading center with uppermost crustal structure features observed at Pito Deep Rift. Basaltic lava flows (thin black lines) dip toward the ridge axis while sheeted dikes (double lines) below commonly dip away from the axis. Faulting, fracturing, and block rotation in the uppermost crust (not shown for clarity) accommodate the thickening of the lava unit to 400 to 500 m within the narrow zone (~1–2 km) of dominant crustal construction.

the amounts of rotation within a geologically plausible sequence of structural rotations. We explore models constructed to fit structural and paleomagnetic data in Area A and B separately.

[37] The bootstrapped mean remanence direction in Area A has a shallower inclination and more clockwise declination than the expected GAD (Figure 13c and Table 2), and as mentioned above, at least two of the three potential structural rotations must have occurred in order to restore the remanence directions. The most recent two structural rotations that could have affected the uppermost crust and contained remanence directions were, in reverse order, related to the block tilting of Pito Deep Rift and rotation of the Easter Microplate. The minimum amount of rotation required by the data is −25.0° ± 15.6° rotation about a horizontal axis (330°/00°) related to block tilting at Pito Deep Rift and vertical-axis (000°/90°) rotation of −33.0° ± 8.1° (Figure 15a). This simple two-stage model restores the observed bootstrapped mean remanence direction back to the GAD expected direction (Table 2); however, this model also results in the average orientation of dikes with strikes to the northeast of the EPR and slight outward dips, away from the EPR axis (034.9°/86.4° SE). A number of different studies indicate that dikes typically intrude perpendicular to the least compressive stress [e.g., *Anderson*, 1951], and in a rift setting dikes are expected to intrude in a nearly vertical orientation near Earth's surface, parallel to the ridge axis (strike parallel to the trend of rift axis with dip approximately 90°) within a very narrow zone (~100s m) centered on the axis. Due to the nearly parallel average dike pole and trend of the horizontal rotation axis related to Pito Deep Rift block tilting, various amounts of rotation result in little change in the average dike orientation, but much larger rotation of the bootstrapped mean remanence direction.

[38] Although the remanence data do not demand any further rotation, the average dike strike of 035° is at least 20° to 25° clockwise from that expected from current rift-axis trends and reconstructions of the EPR axis (010° to 015°). Considerable differences in the strike of dikes near ridge discontinuities such as transform faults or overlapping spreading centers could account for dikes striking obliquely to the regional trend of the spreading axis. However, approximately NNE (~010° ± 5°) bathymetric and magnetic anomaly lineaments for crust of similar age and latitude to the west of the EPR indicate that the ridge axis was oriented ~N/S with no evidence of large discontinuities. This suggests that a greater amount of vertical-axis rotation could restore the average strike of a majority of dikes closer to parallel with the EPR-axial trend. Yet, this greater rotation would also move the bootstrapped mean remanence direction from the expected GAD direction. This change and also the average dip of a majority of the dikes in Area A can both be reconciled by the third suggested rotation about a horizontal axis parallel to the EPR. A best fit three-stage rotation model includes a −21° rotation about a horizontal axis (330°/00°), a −46° rotation about a vertical axis (000°/90°), and an 11° rotation about a horizontal axis (010°/00°). This sequence of rotations restores two modes of dikes in Area A to an initial orientation of 028°/90° for a majority (2/3) of the dikes, 193°/61° NW for the other mode. Whereas the two-stage rotation sequence above is the minimum rotation required by the remanence data, the three-stage rotation sequence restores both bootstrapped mean remanence direction and the average orientation of a majority of dikes to near expected orientations (Figure 15b).

[39] In Area B, a similar two-stage rotation model is the minimum required to restore the bootstrapped mean remanence direction to the expected GAD direction, and includes a −18.0° ± 12.8° rotation about a horizontal axis (330°/00°) and vertical-axis (000°/90°) rotation of −24.0° ± 8.0° (Figure 15c). This simple two-stage model restores the observed bootstrapped mean remanence direction back to the GAD expected direction (Table 2), but similar to the two-stage restoration model for Area A (Figure 15a), also results in orientations of dikes with strikes that are clockwise (northeast) of the expected EPR-axis trend with outward dips, away from the EPR (037.5°/67.3° SE). Although the remanence data do not demand any further rotation, the orientation of the average restored dike in the two-stage model suggests a greater amount of rotation about a vertical axis, and that an additional horizontal-axis rotation could be possible. To reconcile this difference, one best fit three-stage model includes a −10° horizontal-axis (330°/00°) rotation related to Pito Deep Rift block tilting, a −44° vertical-axis (000°/90°) rotation, and a horizontal-axis (010°/00°) rotation of 22° (Figure 15d). This three-stage rotation model restores the bootstrapped mean remanence direction to the expected GAD directions and also the average orientation of dikes in Area B to 013.8°/89.3° SE, nearly vertical (~90° dip) and subparallel to the EPR axis (~010°). To the extent that the ridge-axis rotation occurred about an axis with a trend slightly clockwise from the EPR axis (i.e., >010°), there is a trade-off in associated amount of rotation with the amount of rotation inferred from block tilting at the Pito Deep Rift. That is, the more rotation related to block tilting of Pito Deep Rift, the less rotation that occurred near the EPR axis, and vise versa. The three-stage rotation model suggested for Area B best fits both geological and paleomagnetic evidence for multiple structural rotations of crustal blocks exposed at Pito Deep Rift.

7. Discussion

[40] Exposures at the Pito Deep Rift present the opportunity to investigate one of the only tectonic window perspectives into the oceanic crust created at a superfast spreading ridge; the only other opportunity is at Endeavor Deep Rift. These data illustrate that the complex internal structures of the uppermost oceanic crust generated along the superfast spreading EPR appear to be variations of a reoccurring theme recorded at other fast- to intermediate-spreading environments [*Karson*, 2002]. The documentation of these structural features and associated paleomagnetic remanence directions suggests that structural development poses a significant aspect of uppermost crust deformational history closely associated with crustal accretion at the spreading center. These data also imply significant vertical-axis rotation and support current models for the clockwise rotation of the Easter Microplate. In addition, these results have significant implications for magnetic anomaly intensity and anomalous skewness.

7.1. Shallow Bootstrapped Mean Remanence Directions

[41] The inclinations of bootstrapped remanence directions from both Area A and B are shallower than expected from the GAD by 23.2° ± 15.6° and 15.1° ± 12.8°, respectively, but perhaps they can be explained by other geologic processes or alternative reasons other then rotation. One possibility is that some of the directions included in the mean are from misoriented samples, which could result in a shallower mean inclination. If we arbitrarily suppose that directions of undetermined polarity >44° away from the mean were misoriented, and filter these directions from the bootstrap calculation, the uncertainties on the inclinations from both areas are decreased by almost 6° and although the mean inclination for Area B doesn't change by much more than ~1° (−23.9° ± 7.0), the mean inclination in Area A is ~10° steeper (−27.3° ± 9.9°). This suggests that some of the contribution to shallow bootstrapped mean inclination, particularly in Area A, is from large scatter of the directions; however, even filtering the data does not produce a mean direction with a steeper inclination similar to the expected GAD inclination. Southward motion of the Nazca Plate over the last ~3 Ma contributes to shallower inclinations; however, the contribution of ~0.6° change in latitude suggested from paleomagnetic data from the Galapagos Islands [*Kent et al.*, 2010], corresponds to ~0.8° shallower inclinations and is not sufficient to explain the significant deviation observed. The rotation about a horizontal axis parallel to Pito Deep Rift is one of the only geologically reasonable means of creating more shallow inclinations. Due to the subparallel average dike pole and trend of the horizontal rotation axis related to Pito Deep Rift tilting, large amounts of rotation result in little change in the average dike orientation, but notable change of the bootstrapped mean remanence direction. The amounts of rotation about a horizontal axis parallel to the Pito Deep Rift (330°/00°) required to reconcile the shallow inclinations in the two-stage model are −25° ± 15.6° and −18° ± 12.8° for Area A and B, respectively. However, less amounts of rotation are suggested in the three-stage rotation model with −21° and −10° for Area A and B, respectively. These amounts of rotation are consistent with the ~10°+ backtilt correction inferred from the bathymetry [*Martinez et al.*, 1991], although the amount for Area A is generally greater. If this greater amount of inferred rotation is necessary, then the blocks near Pito Deep may be more tilted than the blocks further east on the Nazca Plate. However, if the shallow inclination is significantly influenced by scatter from some misorientated samples, then it is possible that the amount of tilting at Pito Deep Rift for Area A is less at approximately −13° corresponding to the steeper −27° mean inclination.

7.2. Assessment and Implications of Rotation Models for Area A and B

[42] Bootstrapped mean remanence directions and dike orientations from both Pito Deep Rift study areas deviate from expected orientations, near the GAD direction at 23°S and EPR-axis-parallel strike with vertical dip, respectively. Geological evidence indicates plausible sequential restoration rotation models that include some rift-related horizontal-axis rotation at Pito Deep Rift and vertical-axis rotation related to the Easter Microplate. As a minimum, these two rotations are required to restore the bootstrapped mean remanence directions to the expected GAD direction; however, these two rotations do not restore the strike and dip of the average dikes to expected EPR-axis parallel and vertical orientations.

[43] We suggest both a greater amount of vertical-axis rotation to bring the average strike of dikes subparallel to the expected trend of the EPR axis and a third rotation about a horizontal axis parallel to the EPR to restore the outward dip of dikes to vertical. This three-stage combination of plausible rotations for Area B restores both remanence directions and dike orientations to expected orientations (Figure 15d and Table 2). This third additional rotation is suggested because neither the Pito Deep Rifting (axis near average pole to dikes) nor Easter Microplate (vertical-axis) rotations correct the dip of the dikes to an assumed initial vertical orientation. Data from Area A allow a similar three-stage restoration model to reconcile the average strike of a majority of dikes closer to the EPR-axis trend and vertical dips (Figure 15d and Table 2). Although the overall average dike orientation in Area A is nearly vertical, it is the average of a bimodal distribution of orientations (2/3 of dikes dip SE and 1/3 dip NW). The slight outward dip of a majority of the dikes could be restored to near vertical by the third horizontal-axis rotation parallel to the EPR axis. The third rotation about an EPR-parallel horizontal axis also decreases the dip of the mode of NW-dipping dikes (Figure 15b). Crosscutting relationships in the sheeted dike complex and common dike margin parallel faults at Pito Deep Rift [*Hayman and Karson*, 2009], support this third rotation in both study areas that represents a rotational-planar, or bookshelf, model [e.g., *Mandl*, 1987] and accomplishes the rotation of dikes to their commonly observed outward dips. This mechanism for accommodating block rotations is well documented in sheeted dikes of the Troodos Ophiolite [e.g., *Varga*, 1991] and inferred from dikes at Hess Deep [*Varga et al.*, 2004].

[44] However, if the dikes were intruded into their subvertical orientation and did not rotate at the ridge, Area A does not require a ridge-axis rotation, while Area B more likely requires an additional rotation at the ridge axis. The uncertainty of the average dike orientations is 9.3° and 5.3°, for Area A and B, respectively; however, if we include an additional ~10° uncertainty associated with the Geocompass measurement, then the amount of possible rotation at the ridge axis is approximately near the detectable limit. We cannot exclude the possibility that this ridge axis rotation occurred in Area B, nor do the data necessitate that this rotation occurred in Area A. Perhaps the NW-dipping set of dikes in Area A were not intruded in a vertical orientation, but rather had an initial dip inward toward the ridge axis. The smaller subset of inward-dipping intrusions could have had a more shallow dip, inward toward the ridge axis than observed before inward block tilting at the ridge. Alternatively, these intrusions could have been accreted to the Pacific Plate west of the EPR, tilted inward to produce westerly dip directions, and then transferred to the Nazca Plate east of the EPR by ridge propagation. Another possibility is that this subset of inward-dipping dikes was intruded off-axis, and would have experienced only the two more recent rotations. These two later possibilities would suggest a different tilting history that should be recorded in the remanence directions from this small subset of dikes with inward dip directions, toward the EPR axis. Given the similar remanence directions for both NW- and SE-dipping dikes in Area A and the small number of samples with NW dips, it is possible that some of these dikes had a more shallow dip, inward toward the EPR, which became steeper during subaxial subsidence and inward-tilting of uppermost crustal blocks, or that they were intruded off-axis and only record the two most recent rotations. This set of potential inward-dipping intrusions obviously violates one of the underlying assumptions in the structural rotation models, but appears a probable consequence of the bimodal distribution of dikes.

7.3. Comparison With Other Areas

[45] The most direct oceanic comparison to our observations and data from the northeast wall of Pito Deep Rift derives from studies of crust exposed along the north wall of the Hess Deep Rift. At the Hess Deep Rift, broadly similar uppermost crustal structure expressed by lavas with westerly dips (toward the EPR) and dikes with moderate to steep dips to the east (away from the EPR) are crosscut by steeper, intact, subvertical dikes. Paleomagnetic studies of oriented samples from Hess Deep Rift are compatible with a model in which nonvertical dikes are the result of post-intrusion, structural rotations rather than intrusion in moderately to gently dipping trajectories [*Hurst et al.*, 1994a; *Varga et al.*, 2004]. However, a few differences in uppermost crustal structure were noted between Hess Deep Rift and Pito Deep Rift. Although the geometry and equatorial latitude at Hess Deep makes it very difficult to resolve rotations about N/S, ridge-parallel, horizontal axes, the dikes at Hess Deep have an average dip that is less than at Pito Deep, suggesting that they have been slightly more tilted. This observation, along with qualitatively more cataclastic deformation related to faulting at Hess Deep, indicates a difference in the amount of extension accommodated by faulting compared to dike intrusion as may be expected at a slower spreading rate with less voluminous magmatic activity. Despite these differences, these overall relationships imply that substantial structural deformation took place at uppermost crustal levels within a few kilometers of the EPR axis. This type of complex internal structure has been previously reported [*Karson et al.*, 1992; *Hurst et al.*, 1994a; *Karson et al.*, 2002a; *Varga et al.*, 2004], but the present study documents that it also persists across at least 8 km of the northeast wall exposures of Pito Deep Rift that formed at a (<10%) faster spreading rate than Hess Deep.

[46] Although the remanence directions from oriented samples at Pito Deep Rift do not allow for a unique interpretation of the structural rotations of superfast-spread crust, they do provide some constraints on crustal deformation. A geologically plausible model for the sequence of structural rotations of sheeted dikes exposed in Area B at Pito Deep Rift includes a 22° counterclockwise rotation (right-hand rule) about a ridge-parallel axis (010°/00) to account for the outward dip of the dikes. This amount of rotation is identical to the inferred 22° rotation of a comparable paleomagnetic study at Hess Deep Rift [*Varga et al.*, 2004]. However, the geologically reasonable model for Area A does not require such a large rotation (~11°), if at all. This range of EPR-axis rotation from Areas A and B suggests that dikes are generally less rotated at superfast spreading rates and corresponds to less subaxial subsidence near the ridge axis. The similarity of uppermost crustal structures at Hess Deep and Pito

Deep Rifts and paleomagnetic remanence directions of dikes suggests that similar spreading processes may characterize fast to superfast spreading centers.

[47] At deeper structural levels, massive gabbro exposed at both Pito Deep Rift study areas (Chutas, unpublished thesis, 2007, and J. A. Karson et al., unpublished data, 2005), and at the Hess Deep Rift study area [*Karson et al.*, 2002a; *Varga et al.*, 2004] appears to be less deformed by fracturing than the overlying section at the scale of observation (~10–100s m). Unlike the generally consistent orientations of dikes, no distinct structural features were found within the massive gabbro exposed below the sheeted dike complex. Caution is acknowledged in the interpretation of the limited remanence data for only 8 sites of gabbroic rocks at Hess Deep Rift. However, based on differences between dike and gabbro remanence directions and the observed structural differences within the two units, gabbroic rocks may have deformed under a different mechanism than the overlying crustal units [*Varga et al.*, 2004]. The interpretation of only 5 sites in gabbroic rocks at Pito Deep Rift, are similarly limited, yet a distinct difference in structure between dike and gabbro units is also noted [*Perk et al.*, 2007; Karson et al., unpublished data, 2005; Chutas, unpublished thesis, 2007]. A similarly distinct discontinuity between the gabbros and overlying sheeted dike complex that suggests decoupling and differing styles of deformation has been well documented in the Troodos Ophiolite [*Varga and Moores*, 1985; *Hurst et al.*, 1994b; *Agar and Klitgord*, 1995; *Granot et al.*, 2006], although it likely formed at a different spreading rate.

[48] Further comparison and constraints of mechanical deformation in the uppermost crust are provided by observations and paleomagnetic data from several oceanic drill cores. Most drill cores do not penetrate the entire lava sequence and only a few have recovered sheeted dikes, such as ODP/DSDP Hole 504B and ODP/IODP Hole 1256D. The E/W spreading geometry of 504B is ideal for detecting rotations about ridge-parallel axes with paleomagnetic remanence directions. The dips of chilled margins and paleomagnetic inclinations of sheeted dikes in hole 504B indicate <10° of rotation [*Pariso and Johnson*, 1989; *Allerton et al.*, 1995]. Although the geometry of Hole 1256D is less suitable for determining rotations, the location in superfast-spread crust provides useful comparison to Pito Deep. A range in dip magnitude (~50°–90°) of dike orientations with a mode of ~70°–75° [*Umino et al.*, 2008], and average true dip of ~79° ± 8° NE for chilled margins [*Tominaga et al.*, 2009] suggest that the sheeted dike complex at Hole 1256D is tilted slightly inward, toward the ridge axis by approximately 10–20°. However, drilling-induced remanence and large scatter of paleomagnetic inclinations of the ~350-m-thick sheeted dike unit recovered from Hole 1256D (JANUS database for ODP legs 206 [*Wilson et al.*, 2003], 309, and 312), precludes using remanence data to recognize tilting. Nonetheless, the common observations and measurements of dike margins in drill holes and at tectonic windows demonstrate that dikes are rarely vertical. Currently, few robust sets of paleomagnetic data from drill cores support post-emplacement structural rotations of sheeted dikes. Although some drill core magnetic data suggest structural rotations of the lava unit overlying the sheeted dikes, the scatter of these data and associated uncertainties do not require a systematic change in tilting with depth.

[49] Overall, geologic observations and paleomagnetic data at Pito Deep Rift support models that accommodate subsidence in the uppermost crust (Figure 16). However, data from the Pito Deep Rift suggest that fracture-accommodated rotation of upper crustal units also affects the sheeted dike complex, rather than being confined to the bending and rotation of inward-dipping lavas. This conclusion is in contrast to the interpretation of differential response to post-depositional rotation between the lava unit and underlying sheeted dike complex of 504B and the Akaki River section of the Troodos Ophiolite [*Schouten and Denham*, 2000]. Although that interpretation supports bending and inward-tilting of the lava unit, *Schouten and Denham* [2000] suggest that the underlying sheeted dikes undergo vertical compensation so as to maintain the steep, vertical orientations of the dikes. The common observation of outward-dipping dikes with numerous dike-margin-parallel faults and cataclastic zones in other orientations that both isolate panels of dikes [*Karson et al.*, 2005; *Hayman and Karson*, 2009], suggests that rotational normal ("bookshelf") faulting of panels of sheeted dikes is the dominant mode of deformation and is a significant structural element of the uppermost crust. Dike-parallel slip and associated block rotation are well documented in extensional regimes such as ophiolites [e.g., *Varga*, 1991, 2003]. The outward dip of dikes and inward dip of the lavas suggests that subaxial subsidence plays an important role in accretion of oceanic crust formed at intermediate- to superfast spreading rates. A few, subvertical dikes crosscut panels of variably tilted and fractured dikes and lavas suggesting that block rotations and deformation occurs within the locus of magmatic activity at the spreading center (Karson et al., unpublished cruise report, 2005).

7.4. Constraints on Easter Microplate Rotation

[50] Numerous studies of the bathymetric and magnetic character of the Easter Microplate reveal the details of its tectonic history and evolution [*Hey et al.*, 1985; *Francheteau et al.*, 1988; *Searle et al.*, 1989; *Martinez et al.*, 1991; *Naar and Hey*, 1991; *Rusby and Searle*, 1995]. Many of these studies suggest that the rigid microplate is rotating clockwise at ~15°/Ma [*Rusby and Searle*, 1995], or up to ~17°/Ma to 19°/Ma [*Naar and Hey*, 1991]. Abyssal hill lineaments and magnetic anomalies of the Nazca Plate north/northeast of Pito Deep appear rotated ~20° to >45° clockwise relative to the ~N/S (000° to 015°) oriented fabrics of the Pacific or Nazca Plate crust generated at the EPR. Thus some coupling has occurred between the microplate and adjacent Nazca Plate. Paleomagnetic samples collected from widely spaced dives around and within the Easter Microplate suggest large clockwise rotations [*Cogné et al.*, 1995]. Paleomagnetic data from our study provide a more robust indication of coupling between the Nazca Plate and Easter Microplate [*Varga et al.*, 2008].

[51] The paleomagnetic remanence directions and structural data from the uppermost crust of the Nazca Plate northeast of the Easter Microplate presented in this study support current estimates of clockwise rotation of the Easter Microplate. These data suggest perhaps as much as 44° of clockwise rotation about a vertical axis from a plausible structural model, and indicate a minimum of at least 24°.

These constraints from ~3 Ma crust are entirely compatible with the range of ~15°/Ma to ~18°/Ma of previous models of Easter Microplate rotation [*Naar and Hey*, 1991; *Schouten et al.*, 1993; *Cogné et al.*, 1995; *Rusby and Searle*, 1995; *Varga et al.*, 2008]. It is important to note that these oriented samples from upper crust of the Nazca Plate adjacent to the Easter Microplate show similar rates of clockwise rotation as estimates for rotation of the microplate interior. This amount of rotation and the relatively wide zone of deformation near the northeast microplate boundary implies significant coupling between the clockwise rotating Easter Microplate and the adjacent Nazca Plate. Coupling between the plates supports the assumption that the rapid microplate rotation is driven by coupling along its edges [*Schouten et al.*, 1993].

7.5. Implications for Magnetic Anomalies of Superfast-Spread Crust

[52] The interpretation of linear magnetic anomalies recorded in oceanic crust during accretion plays a fundamental role in determining characteristics of seafloor spreading and in developing and refining the geomagnetic polarity timescale [*Vine and Matthews*, 1963; *Heirtzler et al.*, 1968; *Cande and Kent*, 1995; *Gee and Kent*, 2007]. Basalt lavas of the uppermost crust have historically been considered the primary source of magnetic anomaly lineations [*Smith*, 1990]; however, deeper intrusive units may significantly contribute in many areas [*Gee and Kent*, 2007]. Average magnetization values of ~6 A m^{-1} for dikes at Pito Deep Rift (Table 1) and ~5 A m^{-1} at Hess Deep Rift [*Varga et al.*, 2004], are greater than dikes at Hole 504B (~1.6 A m^{-1}) [*Pariso and Johnson*, 1991], and comparable to values of some lavas collected from oceanic drill cores [*Johnson and Pariso*, 1993; *Gee and Kent*, 2007]. Average predrilling magnetization in the range of 2–5 A m^{-1} from dikes and gabbroic rocks from Hole 1256D [*Teagle et al.*, 2006], are slightly less than dikes at Pito Deep. All of these data suggest that the magnetization of dikes may contribute to observed magnetic anomalies from fast- to superfast-spread oceanic crust. The contribution may be even more significant in oceanic crust with a thinner and/or more extensively fractured and altered lava unit.

[53] Interpretation of the rotation history of dikes from Pito Deep Rift that includes tilting at the EPR axis also has implications for anomalous skewness. Tilting of the magnetic source layers (lavas and dikes) will result in significant anomalous skewness of the observed magnetic anomalies (1° tilt = 1° skewness [*Gee and Kent*, 2007]). The geologically plausible model for Area B includes ~22° inward-tilt of dikes and lavas toward the axis, while Area A does not require a rotation at all, but could have ~11° of inward tilting. This inward tilting would produce anomalous skewness in the opposite sense of that observed at spreading ridges. However, at spreading rates above ~50 km Ma^{-1}, anomalous skewness is not significantly detectable with values within 10° to 15° of zero [*Dyment et al.*, 1994]. If anomalous skewness is not detectable at fast spreading rates, then it is likely that the larger amount of tilt (~22°) is not generally persistent across much of the fast spreading ridge system. Some lesser amount of tilting (~11°) would be more consistent with the range of anomalous skewness values determined from fast-spread crust. Nonvertical polarity boundaries also likely contribute to the skewness of magnetic anomalies [*Tivey*, 1996; *Gee and Kent*, 2007]. If 22° inward-tilt is generally present along the fast spreading ridge system, then the contribution from tilted uppermost crust to anomalous skewness may be balanced by or overcompensated by the skewness contribution from a nonvertical magnetic boundary in the gabbros that dips outward, and away from the spreading axis [e.g., *Gee and Kent*, 2007].

8. Conclusions

[54] Structural observations and paleomagnetic remanence directions from the uppermost oceanic crust exposed at Pito Deep Rift provide new insights into processes of crustal accretion at superfast spreading ridges. These data demonstrate the utility of fully oriented samples from seafloor escarpments in constraining spreading processes. Results from this investigation lead to a number of conclusions regarding magmatic construction and mechanical deformation along the southern EPR, and may have implications for the structure of oceanic crust generated at other fast- to superfast spreading ridges.

[55] 1. Paleomagnetic remanence directions from 62 basaltic dike and 5 gabbroic rock samples, and accompanying structural observations indicate that significant post-intrusion structural rotations have occurred.

[56] 2. Best fit restoration models guided by geological relationships and bootstrapped mean remanence directions incorporate a sequence of three rotations after dike intrusion. First, a rotation about an EPR-parallel horizontal axis, related to subaxial subsidence near the ridge axis to account for the outward dip of the dikes. Second, a rotation about a vertical axis related to the clockwise rotation of the Easter Microplate to account for the northeast strike of the dikes. Third, a rotation about a horizontal axis parallel to the trend of the Pito Deep Rift, related to the block tilting at Pito Deep Rift.

[57] 3. Remanence directions, structural observations, and interpretations indicate that accretion at fast- to superfast spreading ridges involves (>400 m) subaxial subsidence and related inward-tilting between 0° to ~22° rotation of uppermost crustal blocks to accommodate thickening of the lava unit near the spreading axis.

[58] 4. Bootstrapped mean remanence directions and structural data indicate between 44° and 46° of clockwise rotation in the uppermost crust of the Nazca Plate northeast of the Easter Microplate. These data also support estimates from previous studies for clockwise rotation rates of the Easter Microplate of ~11° to 15°/Ma.

[59] 5. Shallow bootstrapped mean remanence directions also suggest ~10° to ~21° rotation about a horizontal axis parallel to the trend of the Pito Deep Rift, related to the block tilting at a propagating rift tip.

[60] 6. The relatively high NRM values of dikes (~6 A/m) and the generally thin lava unit exposed at Pito Deep Rift suggest a significant contribution of the sheeted dikes as a source to magnetic anomalies.

[61] 7. Inward-tilting of uppermost crustal blocks suggested by these data would produce a phase shift (up to −22°) in the skewness of magnetic anomalies, however skewness at fast spreading rates is typically not detectable

(0° ± 15°). This mismatch suggests that inferred inward-tilts of this amount are not persistent along much of the fast spreading ridge system and may not be as general of feature as implied by studies at Hess Deep and Pito Deep Rifts. The amount of inward-tilting, if present, is perhaps typically within the uncertainties of anomalous skewness (≤10° to 15°). Alternatively, the mismatch may reflect that the contribution from nonvertical polarity boundaries in gabbros of the middle to lower oceanic crust balances or overcompensates the contribution of the inward-tilted blocks of uppermost crust.

[62] **Acknowledgments.** We thank the officers and crew of the R/V *Atlantis* and the *Alvin* and *Jason II* pilots and support teams for making our cruise and sampling efforts a success. Our work was supported by NSF grants OCE-0222154 (Karson), OCE-0221948 (Varga), and OCE-0221948 (Gee). Additional thanks to the contribution of the Copeland Fund and Charles B. Moke Prize that supported preliminary undergraduate research (Horst) at the College of Wooster. We also thank our many colleagues who participated and assisted in sampling during the Pito Deep '05 Cruise. We thank Bruce Wilkinson for reviewing an early draft of the manuscript as well as Antony Morris and two anonymous reviewers for comments that improved this manuscript. Special thanks to Lisa Tauxe for development of the free software PmagPy-2.49 used to generate many of the plots in this paper. The Alec Waggoner Memorial Fund has graciously supported a significant portion of publication costs of this paper. This fund was established in loving memory of fellow graduate student Alec Waggoner, with whom the lead author shared enjoyable field trips and passionate geological and universal discussions until his untimely passing.

References

Agar, S. M., and K. D. Klitgord (1995), A mechanism of decoupling within the oceanic lithosphere revealed in the Troodos Ophiolite, *Nature*, *374*, 232–238, doi:10.1038/374232a0.

Allerton, S., and F. J. Vine (1987), Spreading evolution of the Troodos Ophiolite, Cyprus: Some paleomagnetic constraints, *Geology*, *19*, 637–640, doi:10.1130/0091-7613(1991)019<0637:SEOTTO>2.3.CO;2.

Allerton, S. A., A. W. McNeill, L. B. Stokking, J. E. Pariso, P. Tartarotti, F. C. Marton, and N. N. Pertsev (1995), Structures and magnetic fabrics from the lower sheeted dike complex of Hole 504B reoriented using stable magnetic remanence, *Proc. Ocean Drill. Program Sci. Results*, 245–252.

Alt, J. C., et al. (1993), *Proceedings of the Ocean Drilling Program, Initial Reports*, 148 pp., U.S. Gov. Print. Off., Washington, D. C.

Alt, J. C., et al. (1996), Hydrothermal alteration of a section of upper oceanic crust in the eastern equatorial Pacific: A synthesis of results from Site 504(DSDP Legs 69, 70, and 83, and ODP Legs 111, 137, 140, and 148), *Proc. Ocean Drill. Program Sci. Results*, 417–434.

Anderson, E. M. (1951), *The Dynamics of Faulting and Dyke Formation*, 2nd ed., 206 pp., Oliver and Boyd, Edinburgh, U. K.

Anderson, R. N., J. Honnorez, K. Becker, A. C. Adamson, J. C. Alt, M. J. Mottl, and R. L. Newmark (1982), DSDP Hole 504B, the first reference section over 1 km through Layer 2 of the oceanic crust, *Nature*, *300*, 589–594, doi:10.1038/300589a0.

Cande, S., and D. Kent (1995), Revised calibration of the geomagnetic polarity time scale for the Late Cretaceous and Cenozoic, *J. Geophys. Res.*, *100*, 6093–6095, doi:10.1029/94JB03098.

Cann, J. R. (1974), A model for oceanic crustal structure developed, *Geophys. J. R. Astron. Soc.*, *39*, 169–187.

Casey, J. F., J. F. Dewey, P. J. Fox, J. A. Karson, and E. Rosencrantz (1981), Heterogeneous nature of the oceanic crust and upper mantle: A perspective from the Bay of Islands Ophiolite, in *The Oceanic Lithosphere*, edited by C. Emiliani, pp. 305–338, Wiley, New York.

Christeson, G. L., G. M. Purdy, and G. J. Fryer (1992), Structure of young upper crust at the East Pacific Rise near 9°30′N, *Geophys. Res. Lett.*, *19*, 1045–1048, doi:10.1029/91GL00971.

Cogné, J. P., J. Francheteau, V. Courtillot, and P. S. Team (1995), Large rotation of the Easter microplate as evidenced by oriented paleomagnetic samples from the ocean floor, *Earth Planet. Sci. Lett.*, *136*, 213–222, doi:10.1016/0012-821X(95)00191-E.

Delaney, J. R., D. S. Kelley, M. D. Lilley, D. A. Butterfield, J. A. Baross, R. W. Embley, and M. Summit (1998), The quantum event of oceanic crustal accretion: Impacts of diking at mid-ocean ridges, *Science*, *281*, 222–230, doi:10.1126/science.281.5374.222.

Detrick, R. S., A. J. Harding, G. M. Kent, J. A. Orcutt, J. C. Mutter, and P. Buhl (1993), Seismic structure of the southern East Pacific Rise, *Science*, *259*, 499–503, doi:10.1126/science.259.5094.499.

Dyment, J., S. C. Cande, and J. Arkani-Hamed (1994), Skewness of marine magnetic anomalies created 85 and 40 Ma in the Indian Ocean, *J. Geophys. Res.*, *99*, 24,121–24,134, doi:10.1029/94JB02061.

Engeln, J. F., and S. Stein (1984), Tectonics of the Easter plate, *Earth Planet. Sci. Lett.*, *68*, 259–270, doi:10.1016/0012-821X(84)90158-4.

Fisher, N., T. Lewis, and B. Embleton (1987), Statistical analysis of spherical data, 329 pp, Cambridge Univ. Press, New York, doi:10.1017/CBO9780511623059.

Fisher, R. (1953), Dispersion on a sphere, *Proc. R. Soc. London*, *217*(1130), 295–305, doi:10.1098/rspa.1953.0064.

Francheteau, J., P. Patriat, J. Segoufin, R. Armijo, M. Doucoure, A. Yelles-Chaouche, J. Zukin, S. Calmant, D. F. Naar, and R. C. Searle (1988), Pito and Orongo fracture zones: The northern and southern boundaries of the Easter microplate (southeast Pacific), *Earth Planet. Sci. Lett.*, *89*, 363–374, doi:10.1016/0012-821X(88)90123-9.

Francheteau, J., R. Armijo, J. L. Chiminee, R. Hekinian, P. Lonsdale, and N. Blum (1990), 1 Ma East Pacific Rise oceanic crust and uppermost mantle exposed by rifting in Hess Deep (equatorial Pacific Ocean), *Earth Planet. Sci. Lett.*, *101*, 281–295, doi:10.1016/0012-821X(90)90160-Y.

Francheteau, J., R. Armijo, J. L. Cheminee, R. Hekinian, P. Lonsdale, and N. Blum (1992), Dyke complex of the East Pacific Rise exposed in the walls of Hess Deep and the structure of the upper oceanic crust, *Earth Planet. Sci. Lett.*, *111*, 109–121, doi:10.1016/0012-821X(92)90173-S.

Gee, J. S., and D. V. Kent (2007), Source of oceanic magnetic anomalies and the geomagnetic polarity timescale, in *Treatise on Geophysics*, edited by S. Gerald, pp. 455–507, Elsevier Sci., New York, doi:10.1016/B978-044452748-6.00097-3.

Granot, R., M. Abelson, H. Ron, and A. Agnon (2006), The oceanic crust in 3D: Paleomagnetic reconstruction in the Troodos ophiolite gabbro, *Earth Planet. Sci. Lett.*, *251*, 280–292, doi:10.1016/j.epsl.2006.09.019.

Hallenborg, E., A. J. Harding, G. M. Kent and D. S. Wilson (2003), Seismic structure of 15 Ma oceanic crust formed at an ultrafast spreading East Pacific Rise: Evidence for kilometer-scale fracturing from dipping reflectors, *J. Geophys. Res.*, *108*(B11), 2532, doi:10.1029/2003JB002400.

Handschumacher, D. W., R. G. P. Jr., J. A. Foreman, and J. F. Campbell (1981), Structure and evolution of the Easter plate, *Geol. Soc. Am. Mem.*, *1980*, 63–76.

Hayman, N. W., and J. A. Karson (2007), Faults and damage zones in fast-spread crust exposed on the north wall of the Hess Deep Rift: Conduits and seals in seafloor hydrothermal systems, *Geochem. Geophys. Geosyst.*, *8*, Q10002, doi:10.1029/2007GC001623.

Hayman, N. W., and J. A. Karson (2009), Crustal faults exposed in the Pito Deep Rift: Conduits for hydrothermal fluids on the southeast Pacific Rise, *Geochem. Geophys. Geosyst.*, *10*, Q02013, doi:10.1029/2008GC002319.

Heft, K. L., K. M. Gillis, M. A. Pollock, J. A. Karson, and E. M. Klein (2008), Role of upwelling hydrothermal fluids in the development of alteration patterns at fast spreading ridges: Evidence from the sheeted dike complex at Pito Deep, *Geochem. Geophys. Geosyst.*, *9*, Q05O07, doi:10.1029/2007GC001926.

Heirtzler, J. R., G. O. Dickson, E. M. Herron, W. C. Pitman III, and X. Le Pichon (1968), Marine magnetic anomalies, geomagnetic reversals and motions of the ocean floor and continents, *J. Geophys. Res.*, *73*, 2119–2136, doi:10.1029/JB073i006p02119.

Hey, R. N., D. F. Naar, M. C. Kleinrock, W. J. P. Morgan, E. Morales, and J. G. Schilling (1985), Microplate tectonics along a superfast seafloor spreading system near Easter Island, *Nature*, *317*, 320–325, doi:10.1038/317320a0.

Hey, R. N., P. D. Johnson, F. Martinez, J. Korenaga, M. L. Somers, Q. J. Huggett, T. P. LeBas, R. I. Rusby, and D. F. Naar (1995), Plate boundary reorganization at a large-offset, rapidly propagating rift, *Nature*, *378*, 167–170, doi:10.1038/378167a0.

Hey, R. N., F. Martinez, S. Diniega, D. F. Naar, J. Francheteau, and P. D. S. Team (2002), Preliminary attempt to characterize the rotation of seafloor in the Pito Deep area of the Easter Microplate using submersible magnetometer, *Mar. Geophys. Res.*, *23*, 1–12, doi:10.1023/A:1021257915420.

Hooft, E. E., H. Schouten, and R. S. Detrick (1996), Constraining crustal emplacement processes from the variation in seismic layer 2A thickness at the East Pacific Rise, *Earth Planet. Sci. Lett.*, *142*, 289–309, doi:10.1016/0012-821X(96)00101-X.

Hurst, S. D., J. A. Karson, and K. L. Verosub (1994a), Paleomagnetic study of tilted diabase dikes in fast-spread oceanic crust exposed at Hess Deep, *Tectonics*, *13*, 789–802, doi:10.1029/94TC00845.

Hurst, S. D., E. M. Moores, and R. J. Varga (1994b), Structure and geophysical expression of the Solea graben, Troodos ophiolite, Cyprus, *Tectonics*, *13*, 139–156, doi:10.1029/93TC02066.

Johnson, H. P., and J. Pariso (1993), Variations in oceanic crustal magnetization: Systematic changes in the last 160 million years, *J. Geophys. Res.*, *98*, 435–445, doi:10.1029/92JB01322.

Karson, J. A. (1998), Internal structure of oceanic lithosphere: A perspective from tectonic windows, in *Faulting and Magmatism at Mid-Ocean Ridges*, *Geophys. Monogr. Ser.*, vol. 106, edited by W. R. Buck et al., pp. 177–218, AGU, Washington, D. C., doi:10.1029/GM106p0177.

Karson, J. A. (2002), Geologic structure of uppermost oceanic crust created at fast- to intermediate-rate spreading centers, *Annu. Rev. Earth Planet. Sci.*, *30*, 347–384, doi:10.1146/annurev.earth.30.091201.141132.

Karson, J. A. (2005), Internal structure of the upper oceanic crust generated at fast to intermediate rates: The view from tectonic windows in the Pacific, *Eos Trans. AGU*, *86*(52), Abstract T23F-03.

Karson, J. A., S. D. Hurst, and P. Lonsdale (1992), Tectonic rotations of dikes in fast-spread oceanic crust exposed near Hess Deep, *Geology*, *20*, 685–688, doi:10.1130/0091-7613(1992)020<0685:TRODIF>2.3.CO;2.

Karson, J. A., E. M. Klein, S. D. Hurst, C. E. Lee, P. A. Rivizzigno, D. Curewitz, A. R. Morris, and Hess Deep '99 Scientific Party (2002a), Structure of uppermost fast-spread oceanic crust exposed at the Hess Deep Rift: Implications for subaxial processes at the East Pacific Rise, *Geochem. Geophys. Geosyst.*, *3*(1), 1002, doi:10.1029/2001GC000155.

Karson, J. A., M. A. Tivey, and J. R. Delaney (2002b), Internal structure of uppermost oceanic crust along the western Blanco Transform Scarp: Implications for subaxial accretion and deformation at the Juan de Fuca Ridge, *J. Geophys. Res.*, *107*(B9), 2181, doi:10.1029/2000JB000051.

Karson, J. A., et al. (2005), Nested-scale investigation of tectonic windows into super-fast spread crust exposed at the Pito Deep Rift, Easter Microplate, SE Pacific, *InterRidge News*, *14*, 5–8.

Kent, D. V., H. Wang, and P. Rochette (2010), Equatorial paleosecular variation of the geomagnetic field from 0–3 Ma lavas from the Galapagos Islands, *Phys. Earth Planet. Inter.*, *183*, 404–412, doi:10.1016/j.pepi.2010.08.010.

Kent, G. M., A. J. Harding, J. A. Orcutt, R. S. Detrick, J. C. Mutter, and P. Buhl (1994), Uniform accretion of oceanic crust south of the Garrett transform at 14°15′S on the East Pacific Rise, *J. Geophys. Res.*, *99*, 9097–9116, doi:10.1029/93JB02872.

Kirschvink, J. L. (1980), The least-squares line and plane and the analysis of palaeomagnetic data, *Geophys. J. R. Astron. Soc.*, *62*, 699–718.

Larson, R. L., C. T. Popham, and R. A. Pockalny (2005), Lithologic and structural observations at Endeavor Deep and their implications for the accretion process at fast to ultra-fast spreading rates, *Eos Trans. AGU*, *85*(52), Abstract T33D-5094.

Lawrence, R. M., J. A. Karson, and S. D. Hurst (1998), Dike orientations and fault-block rotations in slow-spread oceanic crust at the SMARK Area Mid-Atlantic Ridge at 22°40′N, *J. Geophys. Res.*, *103*, 663–676, doi:10.1029/97JB02541.

Lonsdale, P. (1988), Structural pattern of the Galapagos microplate and evolution of the Galapagos triple junctions, *J. Geophys. Res.*, *93*, 13,551–13,574, doi:10.1029/JB093iB11p13551.

Mandl, G. (1987), Tectonic deformation by rotating parallel faults-the 'bookshelf' mechanism, *Tectonophysics*, *141*, 277–316, doi:10.1016/0040-1951(87)90205-8.

Martinez, F., D. F. Naar, I. T. B. Reed, and R. N. Hey (1991), Three-dimensional SeaMARC II, gravity, and magnetics study of large-offset rift propagation a the Pito Rift, Easter Microplate, *Mar. Geophys. Res.*, *13*, 255–285, doi:10.1007/BF00366279.

Moores, E. M., and F. J. Vine (1971), The Troodos massif, Cyprus, and other ophiolites as oceanic crust: Evaluation and implications, *Philos. Trans. R. Soc. London, Ser. A*, *268*, 443–466, doi:10.1098/rsta.1971.0006.

Naar, D. F., and R. N. Hey (1991), Tectonic evolution of the Easter Microplate, *J. Geophys. Res.*, *96*, 7961–7993, doi:10.1029/90JB02398.

Naar, D. F., F. Martinez, R. N. Hey, I. T. B. Reed, and S. Stein (1991), Pito Rift: How a large-offset rift propagates, *Mar. Geophys. Res.*, *13*, 287–309, doi:10.1007/BF00366280.

Nicolas, A. (1989), *Structure of Ophiolites and Dynamics of Oceanic Lithosphere*, 367 pp., Kluwer Acad., Dordrecht, Netherlands.

Pallister, J. S. (1981), Structure of the sheeted dike complex of the Samail ophiolite near Ibra, Oman, *J. Geophys. Res.*, *86*, 2661–2672, doi:10.1029/JB086iB04p02661.

Pariso, J. E., and H. P. Johnson (1989), Magnetic properties and oxide petrography of the sheeted dike complex in Hole 504B, *Proc. Ocean Drill. Program Sci. Results*, 159–166.

Pariso, J. E., and H. P. Johnson (1991), Alteration processes at Deep Sea Drilling Project/Ocean Drilling Program Hole 504B, *J. Geophys. Res.*, *96*, 11,703–11,722, doi:10.1029/91JB00872.

Penrose Conference Participants (1972), Penrose field conference on ophiolites, *Geotimes*, *17*, 24–25.

Perfit, M. R., and W. W. Chadwick Jr. (1998), Magmatism at mid-ocean ridges: Constraints from volcanological and geochemical investigations, in *Faulting and Magmatism at Mid-Ocean Ridges*, *Geophys. Monogr. Ser.*, vol. 106, edited by W. R. Buck et al., pp. 59–115, AGU, Washington, D. C., doi:10.1029/GM106p0059.

Perk, N. W., L. A. Coogan, J. A. Karson, and E. M. Klein (2007), Primitive gabbroic rocks from a tectonic window at Pito Deep: Implications for the accretion of plutonic rocks beneath the East Pacific Rise, *Contrib. Mineral. Petrol.*, *154*, 575–590, doi:10.1007/s00410-007-0210-z.

Pockalny, R. A., and R. L. Larson (2003), Implications for crustal accretion at fast-spreading ridges from observations in Jurassic oceanic crust in the western Pacific, *Geochem. Geophys. Geosyst.*, *4*(1), 8903, doi:10.1029/2001GC000274.

Pollock, M. A., E. M. Klein, J. A. Karson, and M. A. Tivey (2005), Temporal and spatial variability in the composition of lavas exposed along the Western Blanco Transform Fault, *Geochem. Geophys. Geosyst.*, *6*, Q11009, doi:10.1029/2005GC001026.

Rusby, R. I., and R. C. Searle (1995), A history of the Easter microplate, 5.25 Ma to present, *J. Geophys. Res.*, *100*, 12,617–12,640, doi:10.1029/94JB02779.

Schilling, J. G., H. Sigurdsson, A. N. Davis, and R. N. Hey (1985), Easter microplate evolution, *Nature*, *317*, 325–331, doi:10.1038/317325a0.

Schouten, H., and C. R. Denham (2000), Comparison of volcanic construction in the Troodos ophiolite and oceanic crust using paleomagnetic inclinations from Cyprus Crustal Study Project (CCSP) CY-1 and CY-1A and Ocean Drilling Program (ODP) 504B drill cores, in *Ophiolites and Oceanic Crust: New Insights from Field Studies and the Ocean Drilling Program*, edited by Y. Dilek et al., pp. 181–194, Geol. Soc. of Am., Boulder, Colo., doi:10.1130/0-8137-2349-3.181.

Schouten, H., K. D. Klitgord, and D. G. Gallo (1993), Edge-driven microplate kinematics, *J. Geophys. Res.*, *98*, 6689–6701, doi:10.1029/92JB02749.

Searle, R. C., R. I. Rusby, J. Engeln, R. N. Hey, J. Zukin, P. M. Hunter, T. P. LeBas, H.-J. Hoffman, and R. Livermore (1989), Comprehensive sonar imaging of the Easter microplate, *Nature*, *341*, 701–705, doi:10.1038/341701a0.

Searle, R. C., R. T. Bird, R. I. Rusby, and D. F. Naar (1993), The development of two oceanic microplates: Easter and Juan Fernandez microplates, *J. Geol. Soc.*, *150*, 965–976, doi:10.1144/gsjgs.150.5.0965.

Smith, G. M. (1990), The magnetic structure of the marine basement, *Rev. Aquat. Sci.*, *2*, 205–227.

Soule, S. A., J. Escartín, and D. J. Fornari (2009), A record of eruption and intrusion at a fast spreading axis: Axial summit trough of East Pacific Rise at 9–10°N, *Geochem. Geophys. Geosyst.*, *10*, Q10T07, doi:10.1029/2008GC002354.

Tauxe, L. (2010), *Essentials of Paleomagnetism*, 512 pp., Univ. of Calif. Press, Berkeley, Calif.

Tauxe, L., N. Kylstra, and C. Constable (1991), Bootstrap statistics for paleomagnetic data, *J. Geophys. Res.*, *96*, 11,723–11,740, doi:10.1029/91JB00572.

Teagle, D. H. A., J. C. Alt, S. Umino, S. Miyashita, N. R. Banerjee, and E. a. Scientists (2006), Superfast spreading rate crust 3: A complete in situ section of upper oceanic crust formed at a superfast spreading rate, *IODP Prel. Rep. 312*, doi:10:2204/iodp.pr.312.2006.

Tivey, M. A. (1996), Vertical magnetic structure of ocean crust determined from near-bottom magnetic field measurements, *J. Geophys. Res.*, *101*, 20,275–20,296, doi:10.1029/96JB01307.

Tivey, M. A., H. P. Johnson, C. Fleutelot, S. Hussenoeder, R. Lawrence, C. Waters, and B. Wooding (1998), Direct measurement of magnetic reversal polarity boundaries in a cross-section of oceanic crust, *Geophys. Res. Lett.*, *25*, 3631–3634, doi:10.1029/98GL02752.

Tivey, M., R. Larson, H. Schouen, and R. Pockalny (2005), Downhole magnetic measurements of ODP Hole 801C: Implications for Pacific oceanic crust and magnetic field behavior in the Middle Jurassic, *Geochem. Geophys. Geosyst.*, *6*, Q04008, doi:10.1029/2004GC000754.

Tominaga, M., D. A. H. Teagle, J. C. Alt, and S. Umino (2009), Determination of volcanostratigraphy of oceanic crust formed at superfast spreading ridge: Electrofacies analyses of ODP/IODP Hole 1256D, *Geochem. Geophys. Geosyst.*, *10*, Q01003, doi:10.1029/2008GC002143.

Umino, S., L. Crispini, P. Tartarotti, D. H. A. Teagle, J. C. Alt, S. Miyashita, and N. R. Banerjee (2008), Origin of the sheeted dike complex at superfast spread East Pacific Rise revealed by deep ocean crust drilling at Ocean Drilling Program Hole 1256D, *Geochem. Geophys. Geosyst.*, *9*, Q06O08, doi:10.1029/2007GC001760.

Varga, R. J. (1991), Modes of extension at mid-ocean ridge spreading centers: Evidence from the Solea graben, Troodos ophiolite Cyprus, *J. Struct. Geol.*, *13*, 517–537, doi:10.1016/0191-8141(91)90041-G.

Varga, R. J. (2003), The sheeted dike complex of Troodos ophiolite and its role in understanding mid-ocean ridge processes, in *Ophiolite Concept*

and the Evolution of Geological Thought, edited by Y. Dilek and S. Newcomb, pp. 323–336, Geol. Soc. of Am., Boulder, Colo., doi:10.1130/0-8137-2373-6.323.

Varga, R. J., and E. M. Moores (1985), Spreading structure of the Troodos ophiolite, Cyprus, *Geology*, *13*, 846–850, doi:10.1130/0091-7613(1985)13<846:SSOTTO>2.0.CO;2.

Varga, R. J., J. Gee, L. Bettison-Varga, R. S. Anderson, and C. L. Johnson (1999), Early establishment of seafloor hydrothermal systems during structural extension: Paleomagnetic evidence from the Troodos ophiolite, Cyprus, *Earth Planet. Sci. Lett.*, *171*, 221–235, doi:10.1016/S0012-821X(99)00147-8.

Varga, R. J., J. A. Karson, and J. S. Gee (2004), Paleomagnetic constraints on deformation models for uppermost oceanic crust exposed at the Hess Deep Rift: Implications for axial processes at the East Pacific Rise, *J. Geophys. Res.*, *109*, B02104, doi:10.1029/2003JB002486.

Varga, R. J., A. J. Horst, J. S. Gee, and J. A. Karson (2008), Direct evidence from anisotropy of magnetic susceptibility for lateral melt migration at superfast spreading centers, *Geochem. Geophys. Geosyst.*, *9*, Q08008, doi:10.1029/2008GC002075.

Vine, F. J., and D. H. Matthews (1963), Magnetic anomalies over oceanic ridges, *Nature*, *199*, 947–949, doi:10.1038/199947a0.

Wilson, D. S., et al. (2003), *Proceedings of the Ocean Drilling Program, Initial Reports* [CD ROM], 206. pp., U.S. Gov. Print. Off., Washington, D. C.

Wilson, D. S., et al. (2006), Drilling to gabbro in intact oceanic crust, *Science*, *312*, 1016–1020, doi:10.1126/science.1126090.

A. J. Horst and J. A. Karson, Department of Earth Sciences, Syracuse University, Syracuse, NY 13244-1070, USA. (ajhorst@syr.edu)

J. S. Gee, Scripps Institution of Oceanography, University of California, San Diego, La Jolla, CA 92093-0220, USA.

R. J. Varga, Geology Department, Pomona College, Claremont, CA 91711, USA.